

Review

Theranostics in the vasculature: bioeffects of ultrasound and microbubbles to induce vascular shutdown

Frederic Padilla^{1,2}, Jacqueline Brenner¹, Francesco Prada^{1,3,4}, Alexander L Klibanov^{2,5,6}

1. Focused Ultrasound Foundation, Charlottesville, VA 22903, USA.
2. Department of Radiology, University of Virginia School of Medicine, Charlottesville, VA 22908, USA.
3. Ultrasound Neuroimaging and Therapy Lab, Fondazione IRCCS Istituto Neurologico C. Besta, Milan, Italy.
4. Department of Neurological Surgery, University of Virginia School of Medicine, Charlottesville, VA, USA.
5. Department of Biomedical Engineering, University of Virginia, Charlottesville, VA 22908, USA.
6. Cardiovascular Division, Department of Medicine, University of Virginia, Charlottesville, VA 22908, USA.

 Corresponding author: Frederic Padilla, Focused Ultrasound Foundation, 1230 Cedars Court, Suite 206 | Charlottesville, VA 22903. Phone: 434-220-4993; Email: fpadilla@fusfoundation.org.

© The author(s). This is an open access article distributed under the terms of the Creative Commons Attribution License (<https://creativecommons.org/licenses/by/4.0/>). See <http://ivyspring.com/terms> for full terms and conditions.

Received: 2021.12.22; Accepted: 2023.01.07; Published: 2023.07.14

Abstract

Ultrasound-triggered microbubbles destruction leading to vascular shutdown have resulted in preclinical studies in tumor growth delay or inhibition, lesion formation, radio-sensitization and modulation of the immune micro-environment. Antivascular ultrasound aims to be developed as a focal, targeted, non-invasive, mechanical and non-thermal treatment, alone or in combination with other treatments, and this review positions these treatments among the wider therapeutic ultrasound domain. Antivascular effects have been reported for a wide range of ultrasound exposure conditions, and evidence points to a prominent role of cavitation as the main mechanism. At relatively low peak negative acoustic pressure, predominantly non-inertial cavitation is most likely induced, while higher peak negative pressures lead to inertial cavitation and bubbles collapse. Resulting bioeffects start with inflammation and/or loose opening of the endothelial lining of the vessel. The latter causes vascular access of tissue factor, leading to platelet aggregation, and consequent clotting. Alternatively, endothelium damage exposes subendothelial collagen layer, leading to rapid adhesion and aggregation of platelets and clotting. In a pilot clinical trial, a prevalence of tumor response was observed in patients receiving ultrasound-triggered microbubble destruction along with transarterial radioembolization. Two ongoing clinical trials are assessing the effectiveness of ultrasound-stimulated microbubble treatment to enhance radiation effects in cancer patients. Clinical translation of antivascular ultrasound/microbubble approach may thus be forthcoming.

Keywords: antivascular therapy, ultrasound, cavitation, microbubbles, drug delivery, tumor therapy

1. Introduction

Ultrasound microbubbles (MB) have been investigated for many years for their potential to promote the uptake of drugs into the tumor tissue by exploiting their ability to enhance vascular permeability [1]. Clinical studies are currently exploiting this mechanism to transiently open the blood brain barrier (BBB) for drug delivery [2,3]. Recent publications using either implantable probe [4] or an MRI guided external multi-elements array [5,6] support the generalizability of therapeutic use of ultrasound-activated microbubbles for neuro-oncological applications. These ongoing clinical

studies demonstrate the safety and feasibility of BBB opening, with potential for improved delivery of drugs.

These drug delivery schemes rely on bioeffects following stable, non-inertial cavitation of the microbubbles to induce transient openings of endothelial cell junctions [7]. The more violent effects that can be induced through inertial cavitation, or the violent collapse of the microbubbles [8], have initially been considered as undesirable. It has been reported for more than 30 years that ultrasound can induce capillaries rupture *in vivo* when treatments involve

cavitation such as lithotripsy [9–12], or when driving microbubbles at sufficiently high intensity [13–21], and that even large vessel can be damaged by ultrasound driven microbubbles [22]. It has also been reported that those damages can occur even under diagnostic ultrasound exposures [20,23,24], with in general the pressure amplitude and the MB dose governing the extent of produced bioeffects [25]. Only relatively recently the bioeffects induced by ultrasound exposure of microbubbles have been purposely looked at specifically as therapeutic effects. They have been studied to inhibit tumor growth through a shutdown of tumor blood flow, the induction of non-thermal lesion, or the radiosensitization of tumors when combined with radiotherapy. These anti-vascular effects of ultrasound microbubbles have been reviewed in [26–28].

To our knowledge, three clinical trials are currently being conducted to investigate therapeutic bioeffects induced by microbubbles destruction. The preliminary efficacy results of a pilot clinical trial, using ultrasound-triggered microbubble destruction for radio-sensitization during radioembolization for the treatment of liver cancers, showed a greater prevalence of tumor response in patients receiving both microbubbles and transarterial radioembolization [29]. Two other ongoing clinical trials will assess the effectiveness of ultrasound stimulated microbubble treatment to enhance radiation effects in patients with chest-wall and locally-advanced breast cancer (NCT04431674), or head and neck cancers (NCT04431648).

Various mechanisms have been proposed as the source of therapeutic bioeffects associated with microbubbles destruction by ultrasound. Large range of treatment parameters, including microbubbles doses and sonication regimens, have been reported. The relevance of preclinical findings for the desirable parameters of the respective clinical studies, for the most part, remains an open question.

This review discusses the proposed mechanisms that may explain the observed bioeffects, and tries to elucidate the doses, in terms of microbubbles amount or concentration, and therapeutic ultrasound parameters such as treatment duration or peak acoustic pressure, that are required to induce vascular bioeffects and to promote clinical applications.

The issue of the dose is discussed with regards to possible need for the comparison of the concentrations and quantities of the microbubbles across the studies already published, and relevant metrics to quantify other treatment parameters and responses, such as cavitation monitoring, and ultrasound pulse repetition frequency.

2. Interactions of microbubbles with ultrasound

Before diving into more detailed descriptions of how bioeffects are induced by combined treatment with ultrasound and microbubbles, it is worth reviewing the properties of microbubbles, the ultrasound treatment parameters space and discussing the general mechanism behind the interaction.

Ultrasound microbubbles: Properties, characterization, and recommended dosage

The microbubbles, or ultrasound contrast agents (Figure 1), used in combination with ultrasound to induce vascular bioeffects, are micro-sized gas bubbles coated with a stabilizing layer to provide a compromise between longevity and echogenicity [30,31].

There are currently three FDA approved contrast agents, Lumason, also marketed as SonoVue in Europe (Bracco Imaging SpA, Colliere Giasosa, Italy) composed of a phospholipid monolayer shell and sulfur hexafluoride gas core; Definity (Lantheus Medical Imaging, North Billerica, MA) composed of a phospholipid shell and perflutren gas (C_3F_8 , Octafluoropropane); and Optison (GE Healthcare AS, Oslo, Norway) composed with an albumin shell and perflutren gas (C_3F_8 , Octafluoropropane). In Japan and Korea, a fourth contrast agent is available, Sonazoid (GE Healthcare Inc., Princeton, NJ, USA), which has perfluorobutane gas core and phosphatidylserine shell coating.

The physicochemical characterization of ultrasound agents has been reviewed in the literature (see e.g., [32]), and is summarized in Table 1. The mean diameter in volume is similar for all 3 agents around 8 μm , whereas the diameter in number is slightly higher for Optison (3 μm) than for Lumason (1.9 μm) or Definity (1.22 μm). There is a noticeable disparity between the agents in terms of initial concentration, with Definity more concentrated (84 $\times 10^8$ MB/mL) compared to Optison (7.3 $\times 10^8$ MB/mL) or Lumason (3.4 $\times 10^8$ MB/mL). Caution must be taken when comparing these numbers for different agents, however, as there have been discrepancies in the literature or in the official prescribing information sheets. For instance, in a manuscript that assessed the size distribution of Definity microbubbles[32], it was reported that Definity particle concentration was 1.3 $\times 10^{10}$ MB/mL. The measurement in the latter study was performed with Coulter counter, in the 0.48–12 μm range, so that submicrometer particles could be detected, and dominated the number distribution by an order of magnitude. The prescribing information sheet, “Package Insert”, for Definity microbubbles

lists particle number concentration as 1.2×10^{10} , very close to what was reported in [33]. It is highly likely that particle counting to generate the latter number takes submicron particles into account. Unfortunately, the detailed information on the specific methods and apparatus used to count the microbubbles are not always included within the FDA prescribing information. The presence of very small microbubbles may not be of interest for imaging in the MHz frequency range used in clinics but may be a beneficial source of cavitation nuclei to induce cavitation-related bioeffects.

In terms of a typical injected dose for imaging, there are also significant differences between the agents, both for the injected gas volume (1.65 $\mu\text{g}/\text{kg}$ for Optison and Definity, 0.77 $\mu\text{g}/\text{kg}$ for Lumason) and for the total number of microbubbles/animal weight or MB/kg (12.6 $\times 10^6$ MB/kg for Definity,

5.6 $\times 10^6$ MB/kg for Lumason and Optison). Doses of microbubbles for clinical imaging have been reviewed by Hyvelin et al. [32]. The values for the full clinical doses for bolus injection of the aqueous volume of contrast medium are 34 $\mu\text{L}/\text{kg}$ (2.4 mL/bolus for a 70-kg person) for SonoVue [34], 3 $\mu\text{L}/\text{kg}$ (0.2 mL/bolus for a 70-kg person) for Definity [35], and 15 $\mu\text{L}/\text{kg}$, (1 mL/bolus for a 70-kg person) for Optison [36]. Doses for clinical imaging with microbubbles infusion may differ, and recommended doses are specified in FDA prescribing information notice only for Definity: 1.3 mL, with a rate of infusion initiated at 4.0 mL/minute and not to exceed 10 mL/minute. We should note that the use of the microbubble carrier aqueous medium for dosage should always be accompanied with the particle number concentration, as well as particle gas volume.

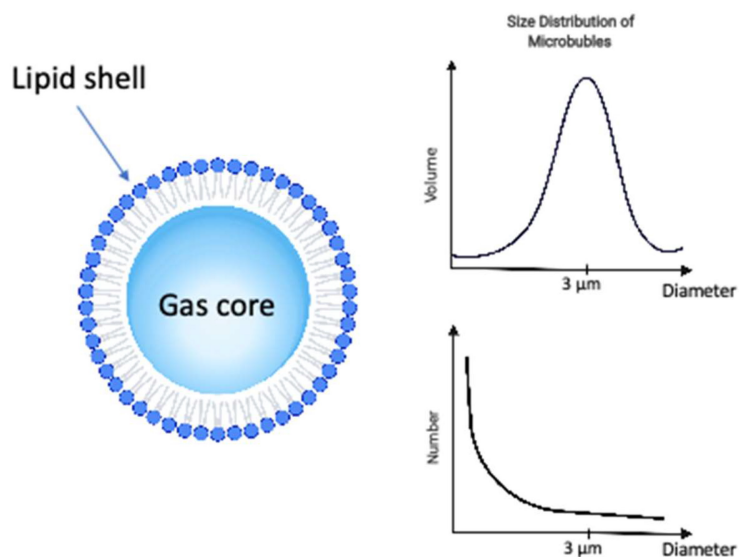


Figure 1: The ultrasound microbubble is composed by a gas core, stabilized by a shell of phospholipid or albumin for the formulations clinically approved for ultrasound contrast imaging. It can be characterized by the composition of its shell, gas core and size distribution among other properties. The distribution microbubbles sizes can be characterized either by the size distribution in volume (top right) or size distribution in number (bottom right), both providing complimentary information.

Table 1: Microbubble properties including composition, size distribution, and clinical dose. Data for mean diameters, concentration, gas volume and microbubble number were adapted from [32].

| Type of Microbubble | Gas Core | Shell composition | Mean Diameter (Volume) | Mean Diameter (Number) | Initial concentration | Injection Gas Volume (typical injected dose) | Total Number Microbubble (typical injected dose) | Full Clinical Dose for Bolus Injection | Other info |
|---------------------|---------------------------------------|-------------------|------------------------|------------------------|-------------------------|--|--|--|--|
| Lumason | sulfur hexafluoride | phospholipid | 8 μm | 1.9 μm | 3.4×10^8 MB/mL | 0.77 $\mu\text{g}/\text{kg}$ | 5.8×10^6 MB/kg | 34 $\mu\text{L}/\text{kg}$ (2.4 mL/bolus for a 70-kg person) | Marketed as SonoVue in Europe (Bracco Imaging SpA, Collioretto Giacosa, Italy) |
| Definity | perflutren (C_3F_8) | phospholipid | 8 μm | 1.2 μm | 84×10^8 MB/mL | 1.65 $\mu\text{g}/\text{kg}$ | 12.6×10^6 MB/kg | 3 $\mu\text{L}/\text{kg}$ (0.2 mL/bolus for a 70-kg person) | Lantheus Medical Imaging, North Billerica, MA |
| Optison | perflutren (C_3F_8) | albumin | 7 μm | 3.1 μm | 7.3×10^8 MB/mL | 1.65 $\mu\text{g}/\text{kg}$ | 5.5×10^6 MB/kg | 15 $\mu\text{L}/\text{kg}$, (1 mL/bolus for a 70-kg person) | GE Healthcare AS, Oslo, Norway |

Ultrasound treatment parameters

Ultrasound waves generated by a transducer are mechanical pressure waves. The properties of these pressure waves and of the ultrasound field will govern the dynamics of the microbubbles' behaviors. An ultrasound treatment sequence is defined by its center frequency, peak rarefactional pressure, also known as peak negative acoustic pressure (PNP), the pulse length (or number of cycles), the repetition frequency of the pulse (or pulse repetition frequency PRF) and the total insonification time. Treatment area can be highly localized, with treatment dimensions down to a few millimeters in diameter when using focused transducer; or can be larger when using focused transducer of a few centimeters in dimensions. The microbubble dynamics will vary depending on several factors including these ultrasound pressure field and exposure conditions, but also depending on the microbubble population characteristics, the local microenvironment and tissue type.

Proposed physical mechanism of ultrasound-microbubbles interaction: Cavitation

Several mechanisms have been proposed to explain observed blood flow disruption in response to insonification of intravascular microbubbles with ultrasound. Although the precise mechanisms responsible for antivascular effects remain uncertain, one prominent candidate is cavitation (Figure 2).

Cavitation refers to the oscillations of microbubbles under the compressional and rarefactional phases of an ultrasound pressure wave [37]. Cavitation can be described as stable or transient. Stable cavitation is usually associated with non-inertial cavitation, where the ultrasound field governs the dynamics of the microbubbles. The microbubbles oscillate until they collapse or fragment [38], or their gas dissolves into

the surrounding fluid [39]. Transient cavitation is generally associated with inertial cavitation, where microbubbles will undergo an unstable expansion phase leading to a rapid collapse dominated by the inertia of the surrounding fluid. Each type of cavitation can induce distinct vascular bioeffects, and will be influenced by the ultrasound field, the microbubbles composition, distribution and concentration and the vascular environment the microbubbles circulate in [40,41].

Inertial cavitation is thought to be a main mechanism of action of microbubbles for vascular damage through violent bubble collapse. It can produce localized regions of high shear stress and temperatures, jetting [42] and an overexpansion or invagination of microvessels [43]. Microvascular damages including hemorrhage, edema and endothelial cell damage and apoptosis [22,40,44,45] have been reported in several tissue types such as tumors and brain. Increased cavitation dose has been linked to increased area of extravasation of red blood cells in the cremaster muscle of rats [46]. Several reports of the presence of inertial cavitation when treating tumors ([47,48] and Table 3) or lesioning normal brain tissue ([49] and Table 4) are consistent with the hypothesis that these phenomena are dominantly associated with inertial cavitation.

Using passive cavitation detector to monitor the onset of inertial cavitation, several studies reported that in the absence of inertial cavitation, vascular shutdowns were not observed (Table 3). Whether these inertial cavitation-induced bioeffects are purely mechanical or thermal in nature cannot be determined from these studies, since it cannot be ruled out that localized temperature elevations occurring in the immediate vicinity of collapsing microbubbles may be occurring [50].

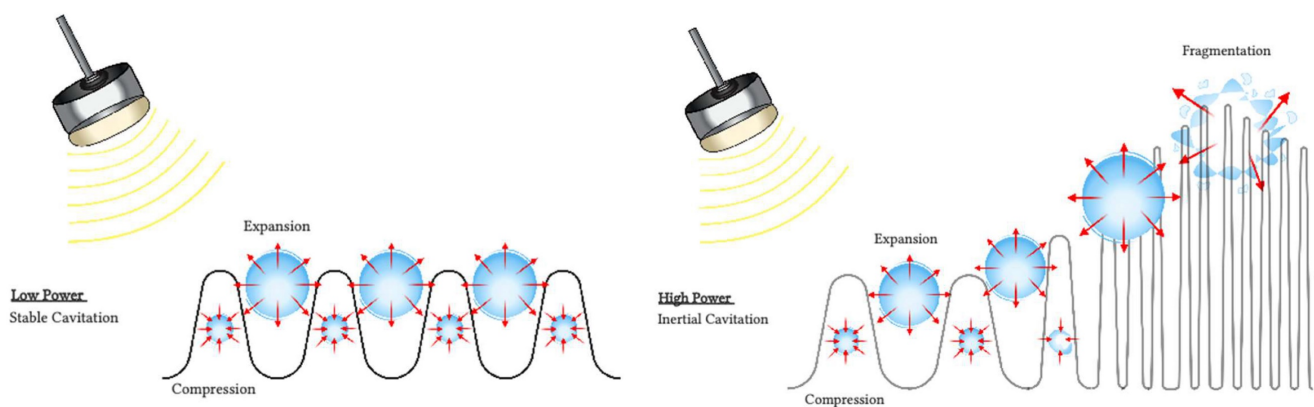


Figure 2: Interactions of microbubbles with ultrasound. During non-inertial cavitation (left), the microbubbles radius oscillates under alternative positive and negative pressures but remains mainly stable overtime. During inertial cavitation (right), the microbubbles radius increases overtime until the microbubble collapses.

Strategies deployed so far to control and sustain cavitation activity rely primarily on the pre-administration of ultrasound contrast agents, shelled microbubbles. The intended effect is mechanical in nature, resulting in bioeffects such as sonoporation or enhancement of vascular permeability. The latter mechanism is the subject of current clinical studies aiming at transiently opening the BBB for drug delivery [4,5]. Monitoring and control of stable cavitation during ultrasound treatment have been reported in preclinical studies of BBB opening, as a reliable tool to ensure maintenance of safe and effective acoustic exposure level [51–53].

3. Applications of ultrasound-microbubbles antivasular treatments

Several applications of ultrasound-microbubbles induced antivasular effects. These include tumor growth control, radiosensitization, mechanical tissue lesioning, modulation of the immune micro-environment. These applications and associated mechanisms are summarized in Tables 3-5 and are discussed in detail in this section.

Tumor growth control

Ultrasound-microbubbles induced vascular flow destruction has been reported to inhibit or delay tumor growth after treatment alone [45,47,54–56], or in combination with chemotherapy [47,48].

Observed tumor growth delays are thought to be the consequence of changes in blood flow, which include either a rapid permanent vascular shutdown or a temporary blood flow shutdown, following microbubbles destruction [45,47,57], as listed in Table 3. Acute complete shutdown of blood flow can occur within seconds after sonication [48] [58]. When sustained, these shut-down of blood flow are followed by widespread apoptosis and necrosis, see for example [45] and Table 3, consistent with ischemia, with the central regions of the tumor being preferentially affected by the exposures. This downstream necrosis of tumor cells is likely responsible for observed decrease in tumor growth, decrease in tumor volumes, and increased survival. Interestingly, even more significant tumor growth inhibition and improved survival was reported when another antiangiogenic medication (cyclophosphamide) was administered in concert with ultrasound- microbubbles induced vascular shut down [47].

Following continuous wave exposures, acute irreparable dilation of the tumor capillaries with associated intercellular oedema were reported, followed by the delayed liquefactive necrosis of

neoplastic cells [59]. The defective construction of tumor neo-vessels can account for their increased vulnerability to the effects of microbubbles destruction. A comparative study in immature and mature vessels revealed that while immature vessels were substantially depleted following microbubbles treatment, both in tumor and in muscle, the mature vessels resisted the effects of treatment in both tissues [55].

As the reduction of blood flow following insonification occurs rapidly, within seconds after ultrasound treatment, potential mechanisms most likely do not involve macrophage recruitment or changes in protein expression.

One proposed model suggests that oscillating microbubbles mechanically damages the endothelium exposing components of the basement membrane including collagen [60], which then causes platelet aggregation and subsequent vessel thrombosis [61] (Figure 3). The platelet aggregation hypothesis was further validated by treating tumors with an anti-CD41 antibody, that binds on the surface of platelets and blocks potential thrombogenic effects, resulting in a greatly decreased reduction in blood flow after sonication [58]. A comparative study in immature and mature vessels revealed that while immature vessels were substantially depleted following microbubbles treatment, both in tumor and in muscle, the mature vessels resisted the effects of treatment in both tissues [55].

There are multiple publications that confirm the link between direct damage to the endothelium and long-lasting vascular shutdown (Table 3). Severe damage to tumor vessels was reported to induce endothelial cells death resulting in vascular depletion and a decrease in tumor perfusion [55].

Damage to the endothelial cells however does not seem to be a prerequisite condition for blood flow shutdown after microbubbles treatment. Several studies reported temporary acute reduction of blood flow or blood flow reduction with blood flow restoration within 5 to 30 minutes after treatment [58,62] (Table 3). These transient reductions of blood flow were not accompanied by obvious structural changes or hemorrhage upon histology. This points to a biological amplification of the relatively limited contact between microbubbles and endothelial cells and suggests mechanisms such as vasospasm.

Several observations of the absence of evidence of coagulation necrosis immediately after microbubbles destruction, although extensive tumor cell necrosis and apoptosis were noted at later time points, suggest that blood flow disruption, and not heating, is the main mechanisms of action [55]. Ultrasound induced thermal mechanisms, such as

thermal ablation, are indeed associated with extensive coagulation necrosis [63,64].

Temperature effects cannot however be completely ruled out. Local temperature changes may occur following cavitation events and enhanced local energy absorption by microbubbles. Depending on treatment parameters, in particular the duty cycle (the fractional ON time), temperature increase due to insonification may be induced. Ultrasound treatment with high duty cycle is known to produce temperature elevation [65,66], while treatment with low duty cycles have not been associated with significant temperature increases (see Table 3). Temperature increases of up to 15°C was measured locally using continuous wave exposures for 3 min [67], of up to 5°C for 1% duty cycle, while no significant macroscopic thermal elevations were recorded at very low duty cycle (0.0001) [45]. Heating arises from absorption of ultrasound energy by viscous damping of the oscillating microbubbles and is influenced not only by the properties of the microbubbles and the sonication parameters, but also by the blood flow, with slower flow leading to higher temperature increase [68].

radiosensitization

A second application of ultrasound-microbubbles induced vascular flow destruction is radiosensitization [69–74]. Vascular shut down is a

critical bioeffect by which radiation induces tumor cell death.

The ability of ultrasound-induced microbubbles destruction to act as a radiosensitizer holds great promise although the optimum protocol for combining two treatments is still unknown. Considerations should guide the timing of the sequence between microbubbles treatment and radiotherapy. One rational suggests that pretreatment with microbubbles can disrupt perfusion and damage tumor endothelial cells resulting in enhanced sensitivity to radiotherapy. Some studies reported optimized sensitization to radiotherapy when microbubbles treatment was performed a few hours before [70,71], whereas others have treated with radiation immediately after microbubbles treatment [75].

Ensuring complete vascular shut down is critical for radiation sensitization as radiation resistance may partly originate from tumor cell hypoxia, allowing cells to metastasize in the presence of reoxygenation. A recurring issue is that lower doses of radiation and other vascular disruptive agents may induce such hypoxia. Complete anoxia rather than hypoxia is desired as complete lack of oxygen results in rapid and complete cell death minimizing the ability for metastatic disease. Therefore, vascular shut down induced by ultrasound-induced microbubbles destruction is an exciting novel antitumor therapy.

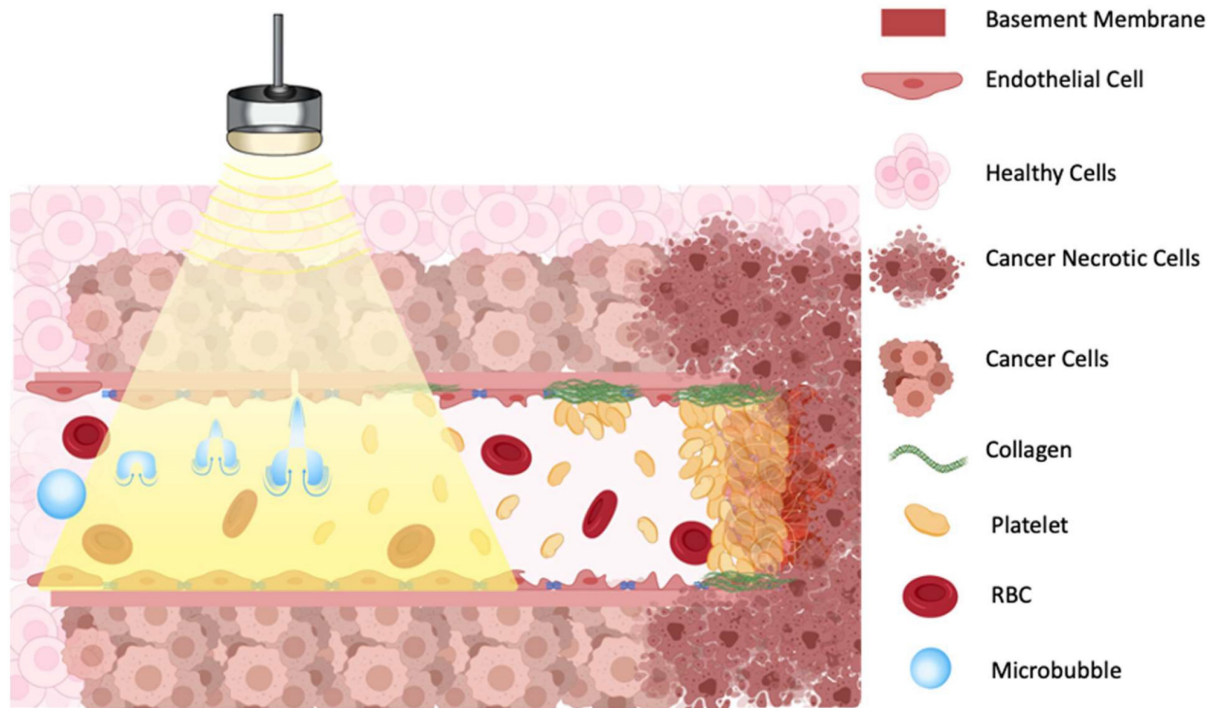


Figure 3: Illustration of proposed mechanism of action on how a combination of microbubbles and Focused Ultrasound damages endothelium, exposing basement membrane and causing aggregation of platelets, resulting in vascular shutdown.

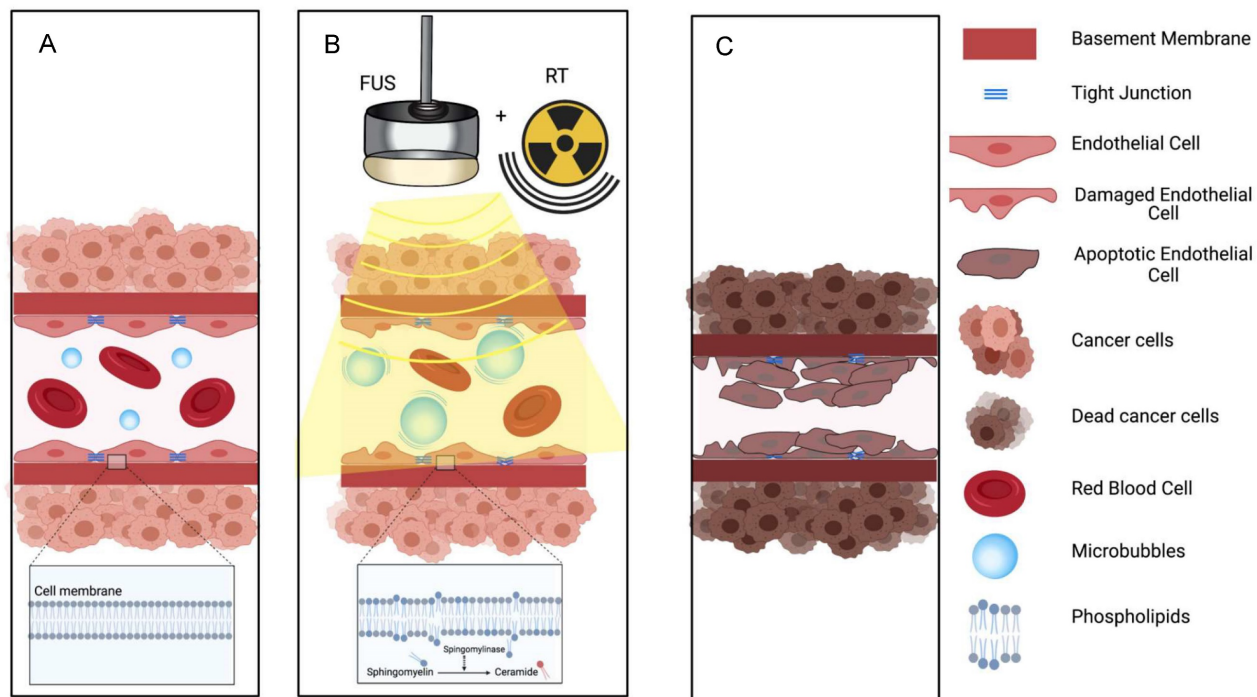


Figure 4: The ceramide model for vascular shutdown with endothelial cell death by ultrasound-induced microbubbles destruction combined with radio-sensitization. A: Injected MB circulates in the blood stream; B: MB destruction by FUS is combined with radiotherapy, causing in ceramide production, and C: resulting in endothelial cell death and subsequent vascular shutdown.

The proposed mechanisms behind ultrasound-microbubbles radiosensitization relies on an evolving theory in radiation oncology that endothelial cell death with vascular shutdown is perhaps more important than the canonical radiation-induced DNA damage for tumor necrosis. This hypothesis is supported by studies where an inhibition of the radiation based vascular responses resulted in minimized treatment response [75,76]. Radiosensitization following vascular shutdown triggered by ultrasound stimulated microbubbles was further enhanced when combined with a blocking antibody against delta-like ligand 4 (Dll4) [77], an angiogenesis deregulator. This triple combination led to a rapid tumor vascular-based collapse and a significant tumor growth delay.

Ultrasound-stimulated microbubbles can cause endothelial cell damage and thrombosis with mechanisms similar to high dose radiation. High dose radiation has been shown to upregulate the amount of ASMase in the endothelium. This converts sphingomyelin into ceramide and induces endothelial cell death and rapid apoptosis. Decreasing the production on ASMase either by pretreating cells with basic fibroblast growth factor (bFGF) or sphingo-1-phosphate (S1P), or by using ASMase deficient mice models resulted in the inhibition of ceramide-induced apoptosis [70]. Endothelial cells also have 20x the amount of ASMase compared to other cells, which leads to a stronger response to

radiation [78]. Treatment with ultrasound and microbubbles can also increase the amount of ASMase [76] and ceramide [70,74,79] leading to endothelial cell death through perturbation of the cell membrane (Figure 4). Increased ceramide staining was demonstrated as early as 1 hour after microbubbles destruction *in vitro* [70]; upregulation of genes that encode sphingomyelinase leads to cell membrane damage and de novo ceramide generation [80]. Because of the known sensitivity of endothelial cell membranes to mechanical forces, the physical effects on endothelial cells induced by microbubbles destruction can interact synergistically with radiation therapy at relatively low (< 6 Gy) as well as at high (> 8 Gy) doses [69,70,73–77,80]. Ultrasound alone or low dose radiation alone are not able to induce vascular shut down [79]. Thus, the combination of ultrasound microbubbles-destruction and low dose radiation could be clinically beneficial, as it may provide an option to avoid high dose radiation, that leads to significant side effects.

Low-intensity pulsed ultrasound treatment, potentially inducing cavitation in the absence of microbubbles, was also shown to activate cell-surface receptors on the endoplasmic reticulum [81].

Modulation of an inflammatory response

While a short-term response is associated with blood flow shutdown, at medium term, inflammatory response following capillary disruption has been

reported to be associated with neo-revascularization, at least in muscle tissues, induced by brief microvascular remodeling response primarily manifested by changes in microvessels [82,83]. The stimulation of expression of cytokines and adhesion molecules following cavitation events has also been used to enhance mesenchymal stem cell homing and engraftment [84,85], to treat myocardial infarction [86,87].

Even following non-inertial cavitation of microbubbles for BBB opening and drug delivery to the brain, acute transcriptional changes in the rat hippocampal microvessels following sonication are indicative of an initiation of angiogenic processes [88]. A modest transient elevation of blood vessel density in the rat hippocampus [89] has been observed. When a high dose of microbubbles was used to open the BBB, using 10x a clinical dose Definity or 100 μ L/kg, an acute inflammation, with activation of the NF κ B signaling pathway and immune activation, including Tnf, Birc3, Ccl2, accompanied by edema, neuronal degeneration, neutrophil infiltration, and microhemorrhage was also observed [90]. BBB opening with microbubbles infusion of 100 μ L of Optison was also reported to be able to induce sterile inflammation, with damage-associated molecular pattern response, concurrent with elevations in proinflammatory, [91] anti-inflammatory, and trophic factors, that lasted for 24 h [92]. These treatments, performed with a high dose of microbubbles, typically 10x higher than the dose used for clinical imaging with Optison, may have resulted in an exaggerated inflammatory response, not observed when optimized parameters are employed.

Lesioning of brain tissues

Initial attempts of using microbubbles destruction to induce brain lesions assumed that microbubbles would enhance the local energy absorption during focused ultrasound exposures [17,93–97]. In fact, time-averaged acoustic power needed to produce localized necrotic lesions in the brain was less than one-tenth compared to the power required to produce thermal lesions without microbubbles in identical experimental conditions [98]. It was also found that the peak temperature was likely not sufficient for thermal damage [99,100]. These results suggest that the low-level heating produced during cavitation was indirectly related to the production of the target lesion at this set of ultrasound parameters. Further studies by the same group demonstrated the formation of lesions in the brain relying on mechanical effects of microbubbles-induced cavitation, without heating [98,101] (Table 4).

When microbubble-induced cavitation is applied to induce lesions in normal brain tissue (Table 4), these lesions are formed presumably via mechanical vascular damage and subsequent ischemia in downstream tissues and localized ischemic necrosis. Lesions are formed with a central region containing red blood cell extravasations surrounded by edema [49]. In the case of brain tissue, however, it is not clear that the mechanically induced damage to the vasculature results in an immediate blood flow shut down. Lesions have been produced while T1w MRI imaging suggested no stop in blood flow just after the treatment [102], while microhemorrhages and lesion formation timeline were consistent with tissue necrosis after ischemic stroke [101]. Histologic findings suggest FUS with microbubbles in the brain might induce two cavitation-mediated processes, ischemia resulting from occlusion of the capillary blood vessels (through the formation of emboli and platelet aggregation) and inducing localized lesions dominated by apoptosis [91], but also potentially some hemorrhagic necrosis [103]. Importantly, animals followed over 9 weeks showed no delayed hemorrhages [101].

Enhancement of response to chemotherapy

Another application of microbubbles destruction is to enhance the effects of chemotherapy by acting as a vascular disruptive agent to destroy the fragile central blood vessels within the tumor and allow for increased delivery of chemotherapy to the tumor periphery [48]. Alternatively, microbubbles destruction can be used to thrombose vessels after targeted drug delivery to enhance drug retention by decreasing washout. microbubbles destruction proved efficacious when coupled with drugs, enhancing anti-tumor effects such as metronomic cyclophosphamide [47] or low-dose docetaxel [48]. Coupling of microbubbles destruction with liposomal doxorubicin (Doxil) had also been proposed, under the rationale that vessel damage and reduction in tumor perfusion resulting from microbubbles destruction would improve intra-tumoral drug uptake [104]. Thus, the effects of vascular shut down to enhance the effects of chemotherapy is likely multifactorial, from destroying intrinsic tumor vessels causing necrosis, to enhancing the efficacy of targeted drug delivery, while also limiting the supply of essential nutrients and oxygen to cells. This approach, involving relatively low acoustic pressures compared to ablation techniques, could be well suited for the treatment of locally advanced tumors, for example in a neoadjuvant context, and could facilitate the treatment of tumors in the brain, kidneys and liver, where acoustic focusing and/or tissue motion can

present challenges for ablative therapy.

Modulation of tumoral immune micro-environnement

Another proposed mode of action of vascular shutdown for antitumor therapy is to trigger an antitumor immune response following endothelial damages. Most preclinical and clinical literature suggests that ultrasound microbubbles destruction may trigger anti-tumor immunity by induction of specific inflammation, modulating immunosuppressive cytokine expression, releasing endogenous danger signals such as heat shock proteins and tumor antigens which can stimulate leukocyte infiltration and activation mostly through increased vascular permeability [105–107]. When low intensity microbubbles destruction was applied to a subcutaneous model of melanoma, there was increased infiltration of HIF1A+ (hypoxia inducible factor 1A+) cells indicative of necrosis and increased CD45+/CD3+ T-cells into the tumors [108]. Similarly, in a subcutaneous mice model of colon carcinoma, non-T regulatory tumor infiltrating lymphocytes and continual infiltration of CD8+ cytotoxic T-lymphocytes with increased CD8+/Treg ratio was reported with low pressure pulsed ultrasound destruction of microbubbles via increased permeability of the vasculature without hyperthermia, and microbubbles destruction had increased antitumor immune response with decreased tumor growth compared to no changes without microbubbles. [109]. However, a more recent study did not observe a shift in T-cell population into a more immunocompetent state when microbubbles destruction was combined with immunotherapy in the later subcutaneous model of colon carcinoma [110]. Such apparent contradictory results may be the consequence of utilizing different US treatment parameters. These studies, indeed, used different treatment settings, pulsed sonications for [110] and continuous sonication for [108], reported to possibly induce hyperthermia [67] at different pressure amplitudes. These elicit different bioeffects, with one treatment resulting in no apparent impact on perfusion but increased vessel permeability and erythrocyte extravasations [109], while the two others resulted in shutdown of blood flow accompanied by necrosis [108,110].

Moreover, analyses of the immune infiltrate were conducted at different time points in these different studies, and the dynamic aspect of an immune-modulation following ultrasound-microbubbles treatment is yet unknown. These reports may also suggest that the exact exposure conditions and associated parameters are of utmost importance in the resulting immunomodulation, as has also been

observed with ablative therapeutic ultrasound modalities [105].

Antitumor immune responses have also been noted with non-ablative ultrasound treatment. In the absence of microbubbles, the treatment of a primary B16 mouse model of melanoma with mechanical focused ultrasound utilizing sufficiently high peak pressure to presumably induce cavitation, was shown to reverse T cell anergy and activate dendritic cells in the tumor and tumor-draining lymph node, with the translocation of surface calreticulin and activation of heat shock proteins (HSPs) which were mechanisms to trigger this immune response [111]. Additionally, treatments with pulsed ultrasound at peak negative pressure of 4 or 6MPa, also likely to be mediated by cavitation, have been reported to modulate an anti-tumor immune response in murine melanoma (B16) and breast (4T1) tumor models, in particular through suppression of anti-inflammatory cytokines [112]. Whether or not similar mechanisms can be activated following microbubbles destruction remains to be studied.

4. Role of treatment parameters

Anti-vascular effects have been reported following a very wide range of exposure conditions, including continuous wave exposure, very short duty cycles, low and high peak negative pressure [43,45,52,53]. The proposed models and mechanisms of action discussed above are summarized in the Table 2. These involve damage to the endothelium, thermal effects and mechanical lesioning. These effects are governed by microbubble dynamics, which in turn will vary depending on several factors including the ultrasound pressure treatment parameters, the microbubble population characteristics, local microenvironment, and tissue type. The role of these treatment parameters is discussed in detail in this section.

Table 2: Summary of antivasular effect and other bioeffects

| Effect | Mechanism |
|-------------------------------------|---|
| Platelet and thrombosis model | MB mechanically damages the endothelium exposing components of the basement membrane, which then causes platelet aggregation and subsequent vessel thrombosis. |
| Ceramide model (Radiosensitization) | MB-induced cavitation increases the amount of ASMase and ceramide production leading to endothelial cell death through perturbation of the cell membrane, and increased sensitivity to radiation. |
| Temperature model | Treatment with long pulse duty cycles results in local temperature elevation, arising from absorption of ultrasound energy by viscous damping of the oscillating MB. |
| Mechanical lesioning model | MB-induced cavitation leads to mechanically induced damage to the microvasculature and direct mechanical tissue lesioning, as well as indirect lesioning by ischemic necrosis. |

Table 3: Antivascular tumors treatment

| Ref. | Animal Model | Microbubbles (MB) | US Exposure Conditions | Biological Effects |
|-------|---|--|---|---|
| [108] | Mice Murine melanoma (K1735) Subcutaneous | Definity, Bolus: 0.2mL Equivalent to 1.7 x10 ⁹ MB or 8.5 x10 ¹⁰ MB/Kg | Physiotherapeutic US machine (D150 Plus; Dynatronics Corp) 3 MHz Unfocused CW for 1 or 3 minutes SATA 2.3 W/cm ² Estimated pressure amplitude 0.22 MPa MI = 0.13 Siemens Sequoia | Significant decrease in the perfused area and in perfusion, treatment-time dependent. Mean decrease in perfusion area of 45% after 1mn of treatment, 67% after 3mn. Focal hemorrhage in area of decreased perfusion, dilated and thrombosed vessels. Presence of local inflammatory response, with increased infiltration of increasing HIF1A+ cells and CD45+CD3+ T cell infiltration in tumors. Tumor blood flow assessed with contrast-enhanced power Doppler (immediately before and after treatment) and Dynamic Contrast-Enhanced MRI (1d before, 5hr after treatment), Reduced regions of blood flow after destructive pulses applied to bound. No flow reduction with flowing MB. Decreasing pulse pressure (4 to 2 MPa) reduced the occurrence of regions of reduced blood flow. |
| [58] | Mice Met-1 or NDL tumors Mammary fat pads | Lipid-shelled MB: targeted (integrin cyclic-RGD or LXY-3 peptide-conjugated) control non-targeted MB Size 2µm Bolus, 10 ⁸ MB Equivalent to 5.10 ⁹ MB/kg | 15L8 transducer, 5 MHz color-Doppler pulses, 8.1 ms pulse repetition period, 6-cycle pulse length, 900 ms insonation 4 MPa or 2 MPa PNP MI = 1.8 | No histological changes in the tumor interstitium, no hemorrhage. Vasculature recovery within 30mn Tumor blood flow alteration assessed by CEUS CPS sequence, histology, platelets binding (50min after treatment) |
| [62] | Mice Murine colon adenocarcinoma (MC38) Subcutaneous | Lipid shell + perfluorobutane Diameter 2 µm Bolus: 2 injections separated by 10mn, 25 x10 ⁸ MB/Kg Equivalent to x100 Definity or x215 Sonovue clinical doses | Philips TIPS device F = 1.2 MHz 3 pulse trains of 10 pulses of 100,000, PRF = 1 Hz Pulse trains separated by a 20 second off period. PNP = 5MPa Effective treatment time = 2.5s (DC 3.5%) | Acute blood flow disruption nearly complete after a single treatment, blood flow returned after about 5-10 minute. Blood flow restoration makes unlikely that vascular endothelium lining were killed acutely, could be vasospasm. No temperature rise recorded during treatment Tumor growth almost completely stopped when daily treatment applied. |
| [45] | Mice Glioma C6 Subcutaneous | Lipid+ decafluorobutane Infusion, 10 ⁸ MB/kg in 0.3mL Equivalent to x1.5 Definity clinical dose (Infusion) | unfocused, 0.75-in-diameter transducer 1MHz 5 bursts of 5000 or 10000-cycles, separated by 50ms OFF Repeated every 5s For 60mn PNP = 1 or 1.2 MHz MI = 1 or 1.2 Effective sonication time = 18 or 36s (DC 0.5 or 1%) | Duty cycle-dependent tumor blood flow reduction immediately after treatment, with perfused area down to 4% (1% DC) of pretreatment flow. Duty cycle-dependent increase in intratumor temperature: +2.5°C for 0.5% DC, +5°C for 1% DC Tumor necrosis and apoptosis significantly increased post-treatment. |
| [47] | Mice nude Breast cancer (human, MDA-MB-231) Hind legs | Definity Bolus, repeated 3 times at 10min intervals 5x10 ⁸ MB/kg (60 µL/kg) Equivalent to x20 Definity clinical dose (single bolus) | focused transducer, 3.75 cm diameter; 15 cm focal length 1MHz Bursts of 50 0.1 ms pulses, spaced 1 ms apart, repeated at 20s intervals For 3 min. PNP at focus 1.65 MPa MI = 1.65 Effective treatment time = 45ms | Acute reduction of perfusion, sustained 24h and 3days after the treatment. Significant growth inhibition following USMB treatment. Combination of antivascular USMB effects with an antiangiogenic therapy (Cyclophosphamide) showed significant growth inhibition and survival prolongation compared to USMB or drug alone. PCD recording shows that inertial cavitation is occurring during the treatment |
| [48] | Mice (nude) Prostate (Human, PC3) Subcutaneous | Experimental MB (Artenga, Ottawa, Canada) Octofluoropropane in sorbitan monostearate (Span 60) and Tween 80 shell, diameter 2.13 µm Bolus, 2.1x10 ⁵ MB/g of mouse weight Equivalent to 2.1x10 ⁸ MB/kg | spherically focused transducer (diameter 3.75 cm; focal length 15 cm) 1 MHz 50 0.1 ms pulses, spaced 1 ms apart, repeated every 20s For 3 mn Repeated 3 times at 10mn intervals PNP 1.65 MPa | Significant 10-fold reduction of flow within the central regions of the tumors, not in the periphery Higher levels of necrosis and apoptosis at 24h Reduction in perfusion staining at 24h, more pronounced in central region of the tumor No improvement in tumor growth control when treatment with MB alone. Significant growth delay and improved survival when treatment with MB+docetaxel PCD recording (single element focused transducer, 750 kHz; focal length 7.5 cm, diameter 2.5 cm, confocally aligned with therapeutic transducer) show that during treatment, subharmonic, ultra-harmonic, and broadband noise are present, associated with MB stable oscillations and inertial cavitation. |
| [110] | Mice colon cell carcinoma | Pegylated phospholipid shells + octafluoropropane (Artenga, Ottawa, | focused transducer, 3.75 cm diameter; 15 cm focal length | Shutdown of blood flow and higher necrosis within the tumors after treatment with US+MB. |

| Ref. | Animal Model | Microbubbles (MB) | US Exposure Conditions | Biological Effects |
|-------|--|---|---|--|
| | (CT26.wt) Subcutaneous, hindlimb | ON, Canada Mean diameter 1-3.7µm Bolus, 9.6x10 ⁸ MB/kg | 1MHz Bursts of 50 0.1 ms pulses, spaced 1 ms apart, repeated at 20s intervals For 2 min. Repeated once after 10min. PNP at focus 1.65 MPa MI = 1.65 | Treatment with US+MB results in delayed tumor growth Treatment with US+MB and aPD1 results in smaller tumors, longer survival time. But absence of evidence by flow cytometry of a shift T-cell subpopulations to a more favorable anti-tumor state. PCD recording (focused 0.75- MHz transducer), show the presence of broadband emissions, a hallmark of inertial cavitation indicating the presence of violent microbubble oscillations during treatment |
| [22] | Rabbit Auricular vein | Optison Bolus, 0.5mL Equivalent to 7.3 x10 ⁷ MB/kg, or x7 Optison clinical dose (single bolus) | focused transducer, 34.9 mm diameter, 5cm focal 1.13 MHz Pulses of 500 cycles PRF 5 Hz (DC =0.22%) For 60s Effective treatment time 132 ms The pulsing sequence started immediately after IV injection of MB | Significant endothelial damage induced in vessels significantly larger (approximately 1 mm diameter) than capillaries Discernable damage (histology) confined to the luminal surface of the blood vessels. No sign of thermal damage to perivascular tissues. |
| [44] | Rabbit Auricular vein | Optison Bolus, 0.5mL Equivalent to 7.3 x10 ⁷ MB/kg, or x7 Optison clinical dose (single bolus) | focused transducer, 34.9 mm diameter, 5cm focal 1.13 MHz Pulses of 500 or 5000 cycles PRF 1HZ (DC 0.04% or 0.4%), For 1 to 120s The pulsing sequence started immediately after IV injection of MB | Significant endothelial damage, resulting in platelet adhesion to the endothelial surface and the formation of an intravascular fibrin thrombus, only in the presence of circulating UCA. Endothelial damage increased with increasing PNP. Higher IC doses correlated with greater endothelial damage TEM images consistent with a mechanical rather than a thermal mechanism of injury to the vascular wall [89] |
| [67] | Mice Melanoma (K173522) Subcutaneous | Definity Bolus, 0.2mL / animal Equivalent to 8.5x10 ¹⁰ MB/Kg or x3400 Definity (single bolus) | Physiotherapy device (D150 Plus, Dynatronics Corp., Salt Lake City, UT, USA) 1 or 3 MHz CW For 3mn PNP =0.27 MPa | Overall reduction of tumor perfusion of 75% at 3MHz. Enhanced reduction of perfusion at 3MHz than 1 MHz. Predominant acute effects = dilation of the tumor capillaries and hemorrhage Temperature increase of 7.8 °C at 1 MHz and 15°C at 3 MHz Because MB were administered in bolus, and since the insonation time used in this study was 180s, it suggests that inertial cavitation may not have been a dominant factor in the observed antivasular effects. But rather relies on thermal effects |
| [54] | Mice Melanoma (K173522) Subcutaneous | Definity Bolus, 0.2mL / animal Equivalent to 8.5x10 ¹⁰ MB/Kg or x3400 Definity (single bolus) | Physiotherapy device (D150 Plus, Dynatronics Corp., Salt Lake City, UT, USA) 3 MHz CW Three 1-min treatments with a 1-min gap between each PNP =0.27 MPa Effective treatment time 3mn | Reduction in tumor growth rate and increased survival time. No monitoring of tumor perfusion changes |
| [55] | Mice Sarcoma (S-180) subcutaneous | Lipid-shelled perfluoropropane microbubbles Bolus, 1.5x10 ⁸ MB/ animal Equivalent to 7.5x10 ⁹ MB/kg | Therapeutic device (KHT-017 transducer, DCT-700, Shenzhen Well.D Medical Electronic, Shenzhen, China). 0.94 MHz PRF 10Hz DC 0.19% 1 min (3s ON, 9s OFF) PNP 0.5, 1.5, 3.0, and 5.0 MPa | Significant decreased perfusion immediately after treatment, sustained at 24h. At 3 MPa, decrease by 84% of blood perfusion and microvessel density of the tumor at 24h. Promoted of tumor cell necrosis and apoptosis, delayed tumor growth, and increased survival rate of tumor-bearing mice |
| [56] | Mice (nude) Pancreatic (XPA-1-RFP) Subcutaneous | Targestar®-P (lipid encapsulated decafluorobutane) 1.9 or 2.9 µm diameter 1x10 ⁸ MB in 70 µl per mouse Equivalent to 5x10 ⁹ MB/kg | Sonicator, 1cm ² tip (Haiying Medical Electronic Instrument Company, Wuxi, China) 238kHz 10ms pulse length DC50% For 60s Repeated 3 successive days 0.5 MPa | Significant reduction in tumor growth compared to control, with both MB sizes. Treatment with 2.9µm MB resulted in more tumor cell necrosis and apoptosis, decreased expression of CD31 and micro-vessel density. |
| [162] | Mice | Perfluoropropane-albumin MB | 3 low-frequency US systems | All parameters tested, sound intensity, frequency, duty cycle, MB |

| Ref. | Animal Model | Microbubbles (MB) | US Exposure Conditions | Biological Effects |
|-------|--|--|---|--|
| | Prostate (PC3) Subcutaneous | (Kangrui Pharmaceutical Co., Yueyang, Hunan, China) 3.4µm diameter Bolus Dose: 0.05, 0.10 or 0.20 ml at 6.5x10 ⁸ MB/mL Equivalent to 1.6 to 6.5x10 ⁹ MB/Kg | (Shanghai Institute of Ultrasound in Medicine, China) 20, 80 and 500 kHz DC 20% (1s ON/4s OFF), 40 (2s ON/3s OFF), or 60% (3s ON/2s OFF) Intensity 0.50, 1.00 or 2.00 W/cm ² For 1, 3 or 5 min | dose, treatment time influenced the decrease in perfusion, with optimal treatment parameters 1 W/cm ² , 20 Hz, DC 40%, MB dose 0.20 ml, treatment time 3 min. Perfusion reduced immediately after treatment, with histology indicating disruption of vascular wall, microvessel dilation, edema in the vicinity[58]f the ruptured vessels No apparent impact on perfusion, as quantified by CEUS after treatment. 2 hr MB treatment, significant increase in vessel permeability, enlarged vascular/cellular or extracellular spaces, with local erythrocyte extravasations, but no apparent increase in apoptotic cells. Significant decrease in tumor volume (18% at 0.6 MPa, and 34% at 1.4 MPa) compared to controls after 16d Local modulation of the immune environment: transient increase in infiltration of non-T regulatory (non-Treg) tumor infiltrating lymphocytes (TILs), continual infiltration of CD8+ cytotoxic T-lymphocytes (CTL), increased CD8+/Treg ratio. |
| [109] | Mice Colon carcinoma (CT-26) subcutaneous | Sonovue Bolus 0.1 mL/kg | Focused transducer (diam 64mm, focus 55mm) 0.5MHz burst length = 100 ms, PFR 1 Hz For 20s 9 to 12 sonications for coverage of the entire tumor PNP 0.6 or 1.4 MP (MI 0.84 or 2) | No apparent impact on perfusion, as quantified by CEUS after treatment. 2 hr MB treatment, significant increase in vessel permeability, enlarged vascular/cellular or extracellular spaces, with local erythrocyte extravasations, but no apparent increase in apoptotic cells. Significant decrease in tumor volume (18% at 0.6 MPa, and 34% at 1.4 MPa) compared to controls after 16d Local modulation of the immune environment: transient increase in infiltration of non-T regulatory (non-Treg) tumor infiltrating lymphocytes (TILs), continual infiltration of CD8+ cytotoxic T-lymphocytes (CTL), increased CD8+/Treg ratio. |
| [163] | Rat Walker carcinoma (Walker 256) Subcutaneous | perfluoropropane encapsulated in lipid shell (DPPG, DSPE) mean diameter of 2 µm Bolus 0.04 mL at 9x10 ¹⁰ /mL. | Focused transducer (25mm diameter, focus 16cm) 831 KHz pulse length of 300cycles, PRF = 1Hz, 6s ON and 6s OFF (DC = 0.0019). Peak pressure: 2.6 MPa or 4.8 MPa | No temperature increase (measured in mimicking phantom using the same FUS exposure energy) Blood flow circulation could be completely blocked off immediately after treatment, for 24 hours in tumors treated at 4.8 MPa, and with a slow recovery starting within 60mn at 2.6MPa Disruption of tumor microvasculature into diffuse hematomas accompanied by thrombosis, intercellular edema and multiple cysts formation. The 24 hours of tumor circulation blockage resulted in massive necrosis of the tumor. |

The references included in the Table are representative of the different treatment schemes proposed to induce vascular flow disruption in tumors. When mentioned, equivalent dose in MB/kg were estimated assuming a 20g mouse. MI = Mechanical Index, PNP = Peak Negative Pressure, PRF = Pulse Repetition Frequency, DC = Duty Cycle, CW = Continuous Wave, SATA = Spatial Average Temporal Average

Table 4: Normal brain lesions

| Ref. | Animal Model | Microbubbles (MB) | US Exposure Conditions | Biological Effects |
|-------|---|--|---|---|
| [49] | Rhesus macaques Normal brains Targets near the skull base | Definity, Bolus: 20 µml/kg (equivalent to 2 times clinical imaging dose) Definity, Infusion: 0.1 ml/min for the first 10 seconds, 0.02 ml/min thereafter | ExAblate MRgFUS 220kHz (InSightec) 220KHz focused 10-msec bursts PRF 1Hz for 5 minutes. Pressure level typically 500kPa, either slightly above or below the cavitation threshold (as assessed by d broadband emissions) | When inertial cavitation present: localized ischemic necrosis, lesions formation with central region containing red blood cell extravasations surrounded by edema, presumably resulting from mechanically induced damage to the microvasculature BBB disruption in the lesions and prefocal area of the FUS system. With bolus injection, a strong inertial cavitation was observed at the start of sonication for about 10 seconds, and then low-level broadband activity With Infusion, a strong inertial cavitation observed was observed sporadically throughout the sonication, with strength of the low-level broadband signal increased over time |
| [102] | Rats Normal brain Transcranial | Definity Bolus 10 or 20 µl/kg Equivalent to 0.85 or 1.7 x10 ⁸ MB or 3.5 or 7 x10 ⁸ MB/Kg | F = 525 kHz 10-msec bursts PRF 1 Hz for 5 minutes PNP estimated at 174 or 195 kPa MI = 0.24 or 0.27 | Lesions produced via destruction of the vasculature and subsequent ischemia in downstream tissues. Damages limited to the endothelium. Ultrasound-induced damage appeared to preferentially affect gray matter structures, more vascularized. T1w imaging suggest that blood flow into the vessels was not stopped. Presumably, these lesions resulted from vascular damage and, in some cases, rupture produced by inertial cavitation, which led to reactive vasospasm, ischemia, and subsequent ischemic necrosis |
| [98] | Rabbit Brain Transcranial | Optison Bolus 0.05 mL/kg Equivalent to 3.65 x10 ⁷ MB/kg or x3.6 Optison clinical dose (single bolus) | Focused transducer, diameter, 10 cm; focal length 8 cm 1.5 MHz 500ms pulse length, PRF 1Hz, For 10 or 20s PNP 2-4MPa | Necrotic lesions, most likely result of cavitation-related damage, time-averaged power to induce lesions was less than one-tenth of what was needed to produce thermal lesions (without microbubbles) and peak temperature remained low. Changes in perfusion were not assessed. |

| Ref. | Animal Model | Microbubbles (MB) | US Exposure Conditions | Biological Effects |
|-------|------------------------------|---|---|--|
| [101] | Rat Brain Transcranial | Optison Bolus 100 µL/kg Equivalent to 7.3.10 ⁷ MB/Kg) or x6.6 Optison (single bolus) | Effective treatment time 5 or 10s FUS 1.1-MHz 10-msec bursts PRF 1 Hz For 300 seconds | Lesions evident immediately after each sonication, presence of microhemorrhages (T2*-weighted images). No delayed hemorrhages. Cystic lesions formed within 2 weeks after sonication stable over time. Results consistent with the timeline with tissue necrosis after ischemic stroke |

The references included in the Table are representative of the different treatment schemes proposed to induce lesion in normal brain using destruction of microbubbles. When mentioned, equivalent dose in MB/kg were estimated assuming a 20g mouse. MI = Mechanical Index, PNP = Peak Negative Pressure, PRF = Pulse Repetition Frequency

Table 5: Radiosensitization: Antivascular effect combined with radiotherapy

| Ref. | Animal Model | Microbubbles (MB) | US Exposure Conditions | Biological Effects |
|------|---|--|--|---|
| [71] | Rats (nude) Hepatocellular carcinoma Orthotopic | Optison Bolus 2.4 x10 ⁸ MB/Kg Equivalent to a x22 clinical dose of Optison (bolus) | Siemens S3000 scanner with 9L4 probe F= 4.2 MHz 1.6 ms pulses PRF 38 Hz for 4s. Repeated 4 times per tumor plane, for a total treatment time of 2-3mn PNP = 2.5 MPa MI = 1.35 Effective treatment time = 0.92s (DC 3%) | Linear decrease of tumor vascularity when the number of destructive sequences increased from 0 to 3. 67% decrease in tumor vascularity after 3 destructive pulses No increase in tumor hypoxia 3 h post treatment (photo-acoustic assessment). When combined with radiotherapy (5Gy single dose), 3hrs after MB treatment, significant improvements in survival time in animals compared to single modality treatment (US of RT), demonstrating a sensitization of tumors to RT. |
| [79] | Mice Fibrosarcoma (MCA-129) Hind leg | Definity Injected during treatment (5mn) 25 µL or 75µL | 500kHz 16-cycle tone burst PRF 3 kHz 5 min PNP 500kPa (MI 0.8) | With MB treatment alone, no significant effect on tumor perfusion, microvascular density, ISEL and ceramide expression at 3, 24, 72 hrs post MB treatment. After radiation, single dose 2 or 8Gy, significant acute reduction in blood flow at 8Gy 3hr after treatment Combined treatment MB destruction and RT (immediately after MB treatment) at 8Gy results in almost 50% decrease in tumor perfusion, peaking at 24h and persisting for up to 72hrs, accompanied by extensive tumor cell death. Use of genetic and chemical approaches demonstrates the role ASMase-ceramide pathway in mechanotransductive vascular targeting using USMB, driving an[56]anced radiation response. |
| [70] | Mice (SCID) Prostate (human PC3) Subcutaneous | Definity 3.6x10 ⁸ or 1.08x10 ⁹ MB (100- and 300-fold diagnostic dose). VEGFR2 targeted MB | Focused single element 500kHz 10% duty cycle within a 50-ms window every 2 s total active insonification time of 750 ms over 5 min for an overall duty cycle of 0.25%. 570kPa (MI 0.76) | Endothelial cell apoptosis induced by MB treatment, and enhanced when combined with RT, leading to a reduction in blood flow and the induction of tumor cell death MB treatment alone maximal effect on blood flow and cell death after 6 h. Greater effect when using VEGFR2-targeted MB MB effects diminished by protection of the vasculature with bFGF Significant reduction of blood flow to tumor treated with the MB destruction and radiotherapy in combination Radiation therapy combined with MB treatment (high concentration) showed effective tumor growth delay at 20d (8Gy single treatment, or 2Gy multiple fraction treatment). Greater survival when MB treatment combined with RT at multiple fraction, with significant effects at non-curative RT dose |
| [75] | Mice, wild-type or asmas knockout (ko) Fibrosarcoma MCA-129 Hind leg | Definity Infusion 25 µL or 77 µL / mice Equivalent to 10 ¹⁰ MB/Kg or 3x10 ¹⁰ MB/Kg x71 Definity (Infusion) X205 Definity (Infusion) Clinical doses | F= 500 kHz 16-cycle tone burst, PFR 3 kHz (DC 1%) For 5 min PNP = 500 kPa MI = 0.71 Equivalent effective treatment time = 3s | Involve ment of ceramide cell death pathway. No statistical effect on tumor perfusion as quantified with 3D power Doppler, with even a trend although non-significant of increased perfusion at 24h with the highest MB concentration used. But decrease in tumor perfusion when US MB destruction combined with radiotherapy treatment. Proposed mechanisms : mechanotransductive vascular targeting of ASMase-ceramide pathway, causing EC death when combined with radiation. |

The references included in the Table are representative of the different treatment schemes proposed to enhance response to radiotherapy via blood flow disruption following microbubbles destruction. When mentioned, equivalent dose in MB/kg were estimated assuming a 20g mouse. MI = Mechanical Index, PNP = Peak Negative Pressure, PRF = Pulse Repetition Frequency, DC = Duty Cycle

Exposure conditions

Antivascular effects have been reported following a very wide range of exposure conditions. Effects have been achieved following continuous wave exposure at low peak negative pressure (or PNP) of about 0.25 MPa [54,67] or very short duty cycles, down to 0.0001 at high PNP (> 1.5MPa). When a range of pulsed-US conditions was examined, it was found possible to induce flow inhibition effects, along with necrosis and apoptosis, using relatively low duty cycles (fractional “on-time” of US; 0.0001–0.01), though the degree of these effects decreased with duty cycle [45]. Vascular shutdown was also reported using very low duty cycle (0.00024) [47].

Two scenarios can therefore be proposed. In the first one, relatively low peak negative pressure is applied, leading to predominantly stable non-inertial cavitation and a dynamic of microbubbles volumetric changes dictated by the ultrasound field. In the second scenario, higher peak negative pressures are applied leading to transient inertial cavitation and bubbles collapse and fragmentation [37,38]. Stable non-inertial cavitation has been associated with transient bioeffects such as increased vascular permeability without endothelial cell damage, necrosis or erythrocytes extravasation [113], although these effects will depend on the acoustic pressure and frequency [60]. Blood-flow or vascular shutdown have been associated with the onset of inertial cavitation [22]. Therefore, the pulsing sequence becomes a primordial parameter to initiate and control the cavitation activity, based on the probability of occurrence and spatial distribution of cavitation, to induce the desired bioeffects.

Ultrasound treatment sequence, defined by its center frequency, peak rarefractional pressure, the pulse length, the repetition frequency of the pulse and the total insonification time, will impact microbubbles dynamic. The ultrasound pulse shape, and especially the peak negative pressure will dictate the microbubbles dynamics on a microsecond scale, with higher pressure levels leading to a shift from stable non-inertial to transient inertial cavitation [38]. However, it is the pulse sequence that will dictate the number of times these dynamics occur and the location where they occur [41]. The shape and sequence of ultrasound pulse have been demonstrated to control magnitudes, types and durations of cavitation events within the focal volume, and a heterogenous distribution of cavitation activity can lead to a heterogeneous distribution of bioeffects [114]. This is especially relevant with long pulses that will result in an upstream destruction of microbubbles flowing into the ultrasound field, inducing an upstream accumulation of cavitation events.

To control the spatiotemporal distribution of acoustic cavitation activity, novel sequences, named rapid short-pulse (RaSP) sequences, based on short pulse sonication (5 to 50 cycles) with short (microsecond order) off-times, were proposed [115]. These RaSP sequences have been shown to improve the lifetime of flowing microbubbles and the spatial homogeneity of cavitation *in vitro* when compared to long pulses of 50000 cycles [115]. When applied to BBB opening in preclinical animal studies, these sequences provided uniform drug distribution in the brain parenchyma [41,116], with optimal BBB opening achieved for series of very short pulses at high PRF (100kHz) repeated at 5Hz [38] or 1.25kHz repeated at 0.5Hz [116]. These RaSP sequences may however require higher dose of microbubbles to be as efficient as longer tone burst sonication to open the BBB [117]. These parametric studies on the influence of ultrasound sequence on the BBB opening may bring very useful lessons for the design of future microbubbles destruction sequences aiming at blood flow or vascular shutdown.

The limit of this comparison however lies in the low PNP used for BBB opening, typically lower than 1MPa [113], at the edge or lower than the inertial cavitation threshold. Whereas the use of short pulses can lead to a higher spatial extent of cavitation events (because of an increased lifetime of flowing microbubbles) - remains to be investigated for PNP of several MPa typically used to induce vascular damages. When violent inertial cavitation is likely to take place, the questions of microbubbles persistence or lifetime, and of the replenishment of the vasculature before the arrival of subsequent acoustic pulses, remain central to the design of ultrasound sequences.

If ultrasound acoustic pressure is sufficiently high for the destruction of microbubbles, PRF may come into play, in relation to blood flow rate in the microvasculature. If acoustic pulse repetition is fast, microbubbles may be destroyed in larger vessels, well before reaching the capillaries, because blood flow in those vessels is relatively slow. If ultrasound pulses are intermittent (e.g., frame rate of 1 Hz is quite common), microbubbles that travel from larger vessels through arterioles may reach the capillaries, before they are destroyed in the bulk blood. At that point, microbubble insonation will lead to bubble expansion to touch endothelium that surrounds the bubble in the capillary. Vessel damage has been reported, even to the point of rupture, RBC leakage, and petechial hemorrhage formation [118].

In the presence of microbubbles, the bio-effects have been achieved with pressure amplitudes lower than would be used in ablative HIFU. Ultrasound

exposure slightly more powerful than diagnostic levels, yet significantly lower than the range used for thermal and ablative treatments, can cause a temporary disruption of tumor blood flow, which can last about ten minutes [62]. The peak pressure however, needs to be above a threshold for microbubbles destruction to occur [119], which will depend on the frequency, the pulse duration, the PRF, the microbubbles type and concentration. When using microbubbles targeting the vascular endothelium, reducing the peak negative pressure decreased the occurrence of regions with reduced blood flow [58]. Studies comparing anti-vascular effects at different pressure amplitude did not report a significant reduction in mean vascular density after treatment at 0.5MPa at 1MHz [55], and no visible damages were observed on the endothelium for pressure below 0.85MPa at 2.25 MHz [46]. Most of the anti-vascular effects by microbubbles destruction were obtained with pressure typically above 1MPa. Although inertial cavitation from ultrasound contrast agents have been reported for peak negative pressure typically starting at 0.5MPa, higher levels of pressure are required to ensure that inertial cavitation is triggered in a significant population of microbubbles, at least for short pulses duration [119]. Studies reporting reduction of tumor perfusion at lower pressure were likely to have been dominated by thermal effects [67].

Microbubbles injection route

Combination of route of administration and selected exposure parameters, especially the PRF, may also be an important factor to induce bioeffects. Comparison of studies performed with similar low duty cycles, show that some induced significant tumor growth delays [47] while some did not [45]. One of the major differences here was the manner of injection, with one study using a large (20s) inter-burst interval to allow microbubbles reperfusion between pulses [47], and the second using shorter inter-burst interval (5s) [45], possibly not long enough to allow replenishment. While no definitive conclusion can be drawn from this comparison because of differences in tumor model and the treatment schedule between these two studies, it can be anticipated that the use of a longer inter-pulse interval should allow replenishment and result in more sustained effects.

When a bolus injection is used, the concentration of microbubbles will vary over time, as evidenced by the dynamic enhancement with contrast-enhanced ultrasound (CEUS) imaging [120]. These variations suggest that over a long treatment period, such as 3min [48] or 60min [45], the induced bioeffects will

decrease over time, if not disappear, and may require multiple microbubbles injections to be sustained. Variation of microbubbles concentration over time also requires a great control over the timing between the microbubbles injection. When microbubbles are injected in bolus, the sonications should typically start a few seconds (15s in [48]) after the start of the injection in order for the microbubbles concentration to reach its peak levels in the region of interest.

In order to optimize treatment efficacy, it is required to ensure that microbubbles are still circulating at the time of the sonication. This can be achieved with an a priori knowledge of microbubbles circulation time and/or real time CEUS imaging. The contrast reperfusion time has been used to determine an optimized timing between burst, such as 20s in [48]. Cavitation monitoring can also be a way to quantify the induced physical effect produced by the insonification of the microbubbles.

Microbubbles dosing

A recent study examined the influence of microbubble parameters, such as size and concentration on BBB disruption. Rats were treated with cationic microbubbles (Advanced Microbubble Laboratories, Boulder, CO, USA composed of DSPC/DSTAP/DSPE-PEG-2K) [121], and sonicated for 5 min (1MHz, 1 MPa PNP, PRF 100Hz, 10%DC) [121]. Using either 2 or 6 μ m diameter microbubbles, and gas volume doses varying from 1 to 40 μ L/kg, it was determined that total gas volume in the administered dose, and not the microbubbles diameter, was the main factor determining the extent of BBB opening, with a linear increase for both diameters.

Whether microbubbles volume could be a unifying parameter in anti-vascular microbubbles ultrasound remains to be investigated. There is also a relationship between microbubbles size and concentration and the persistence in circulation. It has been reported that for matched concentrations, larger microbubbles were more persistent in circulation, but when volume matched, all microbubble sizes had a similar circulation half-life, as evidenced by high-frequency contrast imaging in mice kidney [122].

Generally, microbubbles signal in an intraoperative scan is observed starting from 20-30 seconds after an intravenous bolus injection. In the brain, for example, a complete wash-out depends on the distribution within different areas and tissue types [123,124]. Intravascular lifetime of second-generation ultrasound contrast agents, with a poorly soluble fluorinated gas core, allows the study of structure/organ for several minutes [125]. Circulation times of the clinically approved microbubbles (Sonovue/

Lumason, Optison and Definity) have been described in the literature, in multiple preclinical animal tests and in clinical trial reports of ultrasound contrast imaging blood pool enhancement. They tend to be relatively similar, several minutes following bolus injection or short infusion [126,127]. Contrast enhancement time is prolonged upon the increase of the administered dose (Figure 5). Circulation of second-generation microbubbles agents can be further improved with novel formulations. The BR38 microbubbles from Bracco for example, which incorporates a mixture of perfluorobutane and nitrogen gases, has a body elimination half-life of 10 minutes in humans [128]. Polymer microbubbles such as PBCA (poly(n-butylcyanoacrylate)) may also provide prolonged circulation time [30]. If prolonged insonation treatment is required, bolus administration of microbubbles may be substituted with continuous infusion, which is also an approved technique for contrast ultrasound imaging (see e.g., package insert for Definity or Lumason).

There is an ongoing debate regarding the optimal microbubbles dose, especially for the brain treatment applications. A significant and damaging inflammatory response was observed at high microbubbles doses in preclinical models [90]. But it was also demonstrated that ultrasound with reduced microbubbles dose can induce increased BBB permeability without an associated upregulation of NFκB signaling pathway gene expression [90]. This emphasizes the importance of employing optimized ultrasound parameters and microbubbles dose to mitigate the chances of causing injury to the brain at the targeted locations.

Since there is no regulatory approval for the therapeutic use of microbubbles, we analyzed the preclinical studies based on the FDA-approved doses for diagnostic uses and compared it to a “clinical” dose of microbubbles. To induce downstream

ischemic lesions, the amount of microbubbles used, normalized in terms of number of microbubbles/animal weight, ranged from 10^8 MB/kg when microbubbles are administered in an infusion mode [45] (20x the clinical dose of Definity), up to 10^{10} MB/kg [110] or 10^{11} [108] in bolus for soft tissue applications, which, depending on what microbubbles are used, can represent up to several dozen times the clinical diagnostic dose for a single bolus. For nonthermal ablation of normal brain tissue, localized ischemic necrosis could be achieved with much lower dose, 2- to 6-fold higher than the Optison clinical dose [101]. Postulated mechanisms of the observed bioeffects of microbubble insonation in the vasculature imply that the bubble should be located in close proximity to endothelial lining. Most efficient scenario for the induction of detectable bioeffects implies expansion and compression of microbubbles during insonification cycles, at the time when those bubbles are located within the narrow confines of blood capillaries. In that case, expansion of the bubble during rarefaction will lead to close contact of bubble surface with endothelium, which sometimes leads to deformation of the capillary wall [129]. Obviously, the probability for the bubbles to induce bioeffects will increase with the injected dose of the particles.

Studies using ultrasound-induced microbubbles destruction to induce microvascular damages for radiosensitization used doses much higher than approved for diagnostic imaging purposes. The range was from 2.10^8 MB/kg of Optison (exceeding [55] clinical dose by 22-fold) [71], up to 10^9 MB/kg of Definity, (10- to 300-fold the clinical dose) [70]. Although most studies used high microbubbles doses, treatment parameters optimization is possible to achieve enhanced radiation response with clinically used microbubble concentrations combined with ultrasound [130].

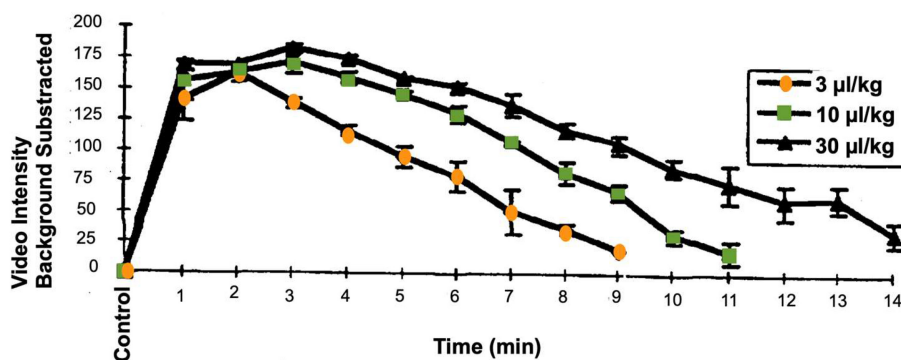


Figure 5: Time-intensity curve for left ventricular opacification and second harmonic imaging in anesthetized dogs, after infusion of Definity microbubbles at different concentration. Each line is the mean \pm SEM (Standard Error of the Mean); N=4; EOI = End of infusion. These data are publicly available on the FDA website, as part of the report “Review and Evaluation of Pharmacology/Toxicology Data” for NDA number 21-064, Definity microbubbles.

These comparisons are difficult because of variations in microbubbles size and compositions (shell and gas), and by other influential ultrasound treatment parameters (frequency, pressure amplitude, DC, PRF, repeated or single treatment) or even the acoustic field (plane v. focused transducers, pressure amplitude). It is notable that achieving microvascular damage through such a wide range of microbubbles concentration can be achieved.

6. Discussion

This review summarizes the current knowledge of ultrasound-induced microbubble destruction to induce antivasular effects. Complete vascular shutdown is the result of cavitation induced microbubbles damage to the endothelial cells either causing platelet aggregation to the exposed basement membranes or via the mechanical activation of the ceramide pathway inducing endothelial cell death and apoptosis. A variety of desired bioeffects can result from antivasular treatment with cavitation alone such as ischemia with tumor necrosis and nonthermal brain lesioning, while in combination with other strategies this treatment can increase radiation sensitization, enhance the effects of chemotherapy, and possibly elicit an anti-tumor immune response. As described in this paper and presented in Tables 3-5, there is significant variability in the ultrasound treatment parameters and the microbubbles administration parameters.

Microbubbles dose and injection routes

In order to safely and effectively induce antivasular effects from cavitation treatments, careful integration of technical focused ultrasound beam parameters and details of microbubbles administration should be considered. For microbubbles, such details include administration mode (intravenous bolus or infusion), time interval between sonications, and microbubbles concentration, size, and composition. The transducer parameters and treatment approach may also be varied, by using manual or electronic steering, quantifying the amount of tumor coverage, and defining pressure settings. In the case of BBB opening, where only transient bioeffects are needed and inertial cavitation is excluded for safety concerns, two different regimens are utilized with either a fixed pressure [4], or an optimization of pressure calculated as 50% of the power at which cavitation signals are first detected using acoustic feedback from an incremental sonication power protocol [52,131]. For other applications, different pressure levels have been used, but in order to induce microbubbles cavitation, pressure levels were typically above 1MPa for

frequencies around 1MHz (Tables 3, 4 and 5) for microvascular ablation, brain tissue lesioning or radiosensitization, or above 0.5MPa for lower frequencies (500kHz); in any case to be above the microbubble's cavitation threshold.

Based on the microbubbles injection mode, timing of ultrasound bursts must be carefully selected to allow reperfusion by microbubbles between two successive pulses. These treatment parameters should also be optimized for specific locations, as microbubbles spatial distribution may greatly vary between organs, and between structures within a given organ such as brain. Pilot studies should be conducted to examine contrast reperfusion time, and a lot can also be learned from ultrasound imaging of microbubbles. In the brain for example, the spatial and temporal distribution of microbubbles is still an area of open investigation, but microbubbles imaging has already provided valuable information. Intraoperative microbubbles contrast-enhancing patterns of intracranial neoplasms have been qualitatively characterized [123,124], with significant differences reported between various subtypes. For example, glioblastoma demonstrated a highly heterogenous and intense pattern of microbubbles, with clearly identifiable arterial suppliers and much faster arterial phase and enhancement peak when compared to lower grade gliomas, which have weaker, more homogenous and slower transit with delayed venous phases. Arterial suppliers and draining vessels are also less clearly visible. Thus, intraoperative differential diagnosis of tumor subtypes (not limited to gliomas) might be achievable through CEUS. Similarly, differences in microbubbles contrast enhancement patterns have been observed between different structures, such as white matter, grey matter, basal ganglia and vascular structures. However, a more standardized, reproducible and quantitative approach would surely be desirable when addressing therapeutic approaches rather than real-time imaging. In this regard, a recent work showed that using time intensity curves for accurate quantitative analysis of microbubbles distribution in CEUS intraoperative imaging enables differentiation of brain tumors as well as variations of flow in different areas of the brain [132]. Such a quantitative approach, once the relation between microbubbles concentration and effects of FUS is established, may allow in the future to optimize treatment outcomes using patient-tailored treatment for maximum therapeutic impact to targets while sparing unaffected areas nearby.

Determining the optimal microbubbles dose in combination with ultrasound beam parameters is critical to mitigate injury at the targeted location.

Since there is no regulatory approval for the therapeutic use of microbubbles, we analyzed the preclinical studies based on the FDA-approved clinical doses of microbubble contrast agents, as prescribed for diagnostic ultrasound imaging. Doses of microbubbles differ greatly between published microbubbles-based anti-vascular studies, as summarized in Tables 3-5 but in general are significantly higher than the amount approved for diagnostic imaging. The amount of microbubbles used, normalized in terms of number of MB/animal weight, ranged from 10^8 MB/kg for infusion [45] which is approximately 20 times the clinical dose of Definity, up to 10^{10} MB/kg [110] or 10^{11} MB/kg [108] as a bolus for soft tissue applications, which can represent more than ten times the clinical dose for a single bolus. For brain applications, localized ischemic necrosis lesioning could be achieved with a much lower dose, only 2 to 6 times the Optison clinical diagnostic dose [101].

When using ultrasound stimulation of microbubbles for BBB opening, a high microbubbles dose using 10x the clinical dose Definity or $100\mu\text{L}/\text{kg}$, elicited acute inflammation with activation of the NF κ B signaling pathway and immune activation, accompanied by edema, neuronal degeneration, neutrophil infiltration, and microhemorrhage [90]. However, safe BBB opening can also be performed without an associated upregulation of NF κ B signaling pathway gene expression by changing protocol settings [90].

Finally, studies using a wide variation of microbubbles doses can induce microvascular damages for radiosensitization ranging from 2.10^8 MB/kg of Optison, or 22 times the clinical dose [71], up to 10^9 MB/kg of Definity, 10 to 300 times the clinical dose [70]. These comparisons are difficult to interpret because of variations in microbubbles size, composition (shell and gas), and other technical factors in the US beam properties.

Timing of ultrasound microbubbles destruction treatment with combination therapies

If drugs are used in association with microbubbles treatment, their pharmacokinetic properties are a crucial factor to determine the timing of their injection. Injection of drugs before microbubbles allows enhanced drug penetration within the tumors. Time interval between drug injection and microbubbles treatment must be carefully selected with respect to the drug plasma half-time, to avoid situations where microbubbles treatment would start too late, after the drug has already been cleared from plasma.

Same considerations should guide the timing of the sequence between microbubbles treatment and radiotherapy when used in association. One rational for this association is that pretreatment with microbubbles can disrupt perfusion and damage endothelial cells in tumors, resulting in enhanced sensitivity to radiotherapy. The time interval between microbubbles treatment and radiotherapy should take into consideration the dynamics of perfusion shutdown. This time interval is not yet standardized as some studies reported optimal sensitization to radiotherapy with microbubbles administration a few hours before [70,71] or immediately after microbubbles treatment [75]. A recent study evaluating multiple time intervals with ultrasound microbubbles destruction before and after radiation, suggested vascular normalization as a consequence of a combinatorial therapy [133].

Novel applications of intravascular ultrasound-microbubble treatments

Novel applications of microbubbles-microvascular bioeffects that induce vascular shut down are being proposed. Simulating the spatial resolution of a laser to precisely nucleate bubbles in selected vessels, synchronized with an acoustic pulse (1 MHz at 0.45 MPa and 10 Hz with 10% duty cycle), was recently reported to induce an almost 70% reduction in blood perfusion after 7 days in a rabbit ear model, without damaging the surrounding cells [134]. The combination of tumor microvascular injuries and embolization with sonodynamic therapy using berberine (BBR) nanoparticles as a sonosensitizer demonstrated suppression of tumor proliferation [135]. Another use of microbubbles-induced cavitation has also been studied to improve atherosclerotic plaque stability by selectively destroying the intraplaque neovasculature with a treatment at 3MPa through a reduction in erythrocyte extravasation and inflammatory mediator influx [136]. Destruction of microbubbles was also used to deliver IL-8 monoclonal antibodies in a rabbit model of atherosclerotic plaques and was shown to alleviate inflammation [137].

Interestingly, microbubbles destruction is now investigated as an adjunct to microwave ablation. The significantly reduced tumor blood perfusion can lead to a sharp rise in the local temperature of the treatment area, resulting in increased necrosis and apoptosis in a murine model of hepatocellular carcinoma (HCC) [138].

Other potential clinical use of microbubbles focused ultrasound is to enhance vascular permeability and cell transfection in the brain. For example, significant preclinical studies have

demonstrated the ability of low intensity focused ultrasound to enable liquid biopsy in the brain by opening the blood brain barrier. Following treatment of brain tumors in mice with pulsed ultrasound and microbubbles (1.5MHz, 1.5MPa, pulse length 10 ms, PRF pulse, for 30 s at 4 different locations), an increase of up to 4800-fold in a reporter mRNA (eGFP) was found in the peripheral blood samples compared to untreated mice [139]. Follow-up studies in small and large animals with MRI imaged guided brain-tumor biomarker release confirmed the efficacy and the safety of the technique [140,141]. A proof-of concept study reported the ability of MRgFUS to enhance the release of circulating brain-derived biomarkers including cfDNA, extracellular vesicles, and brain specific protein, demonstrating the potential of the technology to support liquid biopsy for the brain [142].

Activation of cationic microbubbles coated with plasmid DNA microbubbles with very low-pressure focused ultrasound (0.1 MPa, 1.1 MHz) selectively and effectively delivered genetic material to the targeted cerebral microvessels in mouse brain, without disrupting blood-brain barrier integrity or eliciting detectable inflammation, opening novel perspectives in sono-selective transfection [143].

The destruction of microbubbles at the reduced acoustic power levels with magnetic resonance imaging (MRI)-guided focused ultrasound (MRgFUS) was reported as a tool to achieve mild hyperthermia. When combined with liposomal doxorubicin (Caelyx), this hyperthermia resulted in increased levels of drug in muscle but not tumor tissue, suggesting a complex interplay between the heating effects of microbubbles with those of enhanced permeabilization and possible vascular damage in the tumor [144].

An interesting example of microbubbles-mediated bioeffects outside the brain is related to sonoporation and increased vascular permeability for enhanced drug delivery. It has been applied in an early-stage clinical trial with encouraging results to deliver gemcitabine in pancreatic tumor of inoperable patients [145], and there is a plethora of preclinical data [8,146].

Perhaps one method of improving the ability to control cavitation induced vascular shut down involves exploring the use of other agents that can also interact with ultrasound to induce cavitation-related bioeffects. Acoustically activated droplets, also known as phase-change emulsion [147] droplets, can vaporize under ultrasound stimulation [148]. They can be potentially used with spatial and temporal control resulting in targeted tissue occlusion [149,150]. Novel agents, such as an ultrasound-

responsive single-cavity polymeric nanoparticle, has been recently shown to actively transport and improve the distribution of therapeutic agents in tumors [149,151], and can enable the extensive extravasation at low acoustic energies [152]. To our knowledge, these agents have not yet been investigated for anti-vascular therapy. They can present some potential advantages over microbubbles, such as longer circulation time, and capacity to extravasate.

Imaging for treatment planning and monitoring

All these treatments are intrinsically linked to imaging for treatment planning, targeting, monitoring and follow-up. Ultrasound imaging seems the most natural imaging modality, as it can monitor blood tissue perfusion and blood velocity in the vessels, especially when enhanced by microbubble contrast for imaging or for microbubble-enhanced Doppler [153]. Microbubbles contrast imaging is for example used to assess tissue destruction following thermal treatment with high intensity focused ultrasound (HIFU) of prostate cancer [154,155]. This imaging is performed while the patient is still in the operating room, so immediate re-treatment is possible in case of an unsatisfactory result, demonstrating that the unwanted bioeffects of microbubbles in a therapeutic ultrasound setting can also be safely mitigated.

More recently developed modalities of ultrasound imaging have open prospects for a detailed characterization of vessel morphology and blood flow characterization. Two proposed methodologies have pushed the limits of what is achievable in terms of imaging resolution of blood vessels with ultrasound. The first one, named acoustic angiography, is a dual-frequency contrast-enhanced technique, using a regular emission frequency (a few MHz) for excitation of microbubbles, and a very high receiving frequency (typically between 10 and 20 MHz) for constructing images with a better resolution than otherwise achievable with a single transmit-emit frequency. When implemented with dedicated transducers and image processing, this method can generate images with a resolution down to a few tens of microns [156–158]. The second approach, named super-resolution imaging, relies on specific ultrafast acquisition techniques and post-processing, to image at resolutions beyond the wavelength limits of the device. Several postprocessing algorithms for CEUS image analysis have recently been proposed for a detailed characterization and quantification of vascular features at super-resolution [159–161], and could also open novel ways to plan and monitor treatment response.

Clinical translation

With the knowledge gleaned from the preclinical work with ultrasound vascular ablation, researchers at Thomas Jefferson University recently published the results of the first pilot clinical study using ultrasound-triggered microbubbles destruction for augmenting hepatocellular carcinoma response to transarterial radioembolization (NCT 03199274) [29]. There was a greater prevalence of tumor response in participants who received a combination treatment, i.e., ultrasound-triggered microbubbles destruction and radioembolization versus radioembolization alone, with no significant complications. The patients receiving both treatments received 3 separate microbubbles destruction sessions 1-4 hours and approximately 1 and 2 weeks after radioembolization. An ultrasound triggered microbubbles destruction sequence was used with a mechanical index of 1.13 at 1.5MHz transmitting at 2.3 μ sec pulses and a PRF of 100Hz and repeated for several minutes [27]. Two other clinical trials that use ultrasound microbubbles destruction for radiosensitization for head and neck cancers (NCT04431648) and chest-wall/locally-advanced breast cancers (NCT04431674) are currently recruiting patients.

7. Conclusion

Ultrasound-induced microbubbles destruction antivasular effects can potentially be utilized as a focal, targeted, noninvasive treatment, alone or in combination with other treatments. Additional knowledge gaps should be investigated to allow further advancements and allow for increased translational research. It is likely that this treatment modality will bring more clinical trials, when the questions of ultrasound treatment parameters and microbubbles dose will have been optimized.

Competing Interests

A. Klivanov declares that he is a co-founder and minority shareholder of Targeson Inc, a startup in the area of preclinical targeted contrast ultrasound microbubbles (now dissolved); his UVA lab is also a recipient of an NIH grant subcontract via SoundPipe Therapeutics (Charlottesville VA). Other authors have declared no competing interests.

References

- Snipstad S, Sulheim E, Davies C de L, Moonen C, Storm G, Kiessling F, et al. Sonopermeation to improve drug delivery to tumors: from fundamental understanding to clinical translation. *Expert Opin Drug Deliv.* 2018; 15: 1249-61.
- Song K-H, Harvey BK, Borden MA. State-of-the-art of microbubble-assisted blood-brain barrier disruption. *Theranostics.* 2018; 8: 4393-408.
- Liu H-L, Fan C-H, Ting C-Y, Yeh C-K. Combining microbubbles and ultrasound for drug delivery to brain tumors: current progress and overview. *Theranostics.* 2014; 4: 432-44.
- Carpentier A, Canney M, Vignot A, Reina V, Beccaria K, Horodyckid C, et al. Clinical trial of blood-brain barrier disruption by pulsed ultrasound. *Sci Transl Med.* 2016; 8: 343re2-343re2.
- Mainprize T, Lipsman N, Huang Y, Meng Y, Bethune A, Ironside S, et al. Blood-Brain Barrier Opening in Primary Brain Tumors with Non-invasive MR-Guided Focused Ultrasound: A Clinical Safety and Feasibility Study. *Sci Rep.* 2019; 9: 987-7.
- Abraham A, Meng Y, Llinas M, Huang Y, Hamani C, Mainprize T, et al. First-in-human trial of blood-brain barrier opening in amyotrophic lateral sclerosis using MR-guided focused ultrasound. *Nat Commun.* 2019; 10: 4373.
- Mo S, Coussios C-C, Seymour L, Carlisle R. Ultrasound-enhanced drug delivery for cancer. *Expert Opin Drug Deliv.* 2012; 9: 1525-38.
- Stride EP, Coussios CC. Cavitation and contrast: the use of bubbles in ultrasound imaging and therapy. *Proc Inst Mech Eng H.* 2010; 224: 171-91.
- Dalecki D, Raeman CH, Child SZ, Carstensen EL. Intestinal hemorrhage from exposure to pulsed ultrasound. *Ultrasound Med Biol.* 1995; 21: 1067-72.
- Dalecki D, Raeman CH, Child SZ, Carstensen EL. Thresholds for intestinal hemorrhage in mice exposed to a piezoelectric lithotripter. *Ultrasound Med Biol.* 1995; 21: 1239-46.
- Dalecki D, Raeman CH, Child SZ, Carstensen EL. A test for cavitation as a mechanism for intestinal hemorrhage in mice exposed to a piezoelectric lithotripter. *Ultrasound Med Biol.* 1996; 22: 493-6.
- Miller DL, Thomas RM. Thresholds for hemorrhages in mouse skin and intestine induced by lithotripter shock waves. *Ultrasound Med Biol.* 1995; 21: 249-57.
- Dalecki D, Raeman CH, Child SZ, Penney DP, Mayer R, Carstensen EL. The influence of contrast agents on hemorrhage produced by lithotripter fields. *Ultrasound Med Biol.* 1997; 23: 1435-9.
- Dalecki D, Child SZ, Raeman CH, Xing C, Gracewski S, Carstensen EL. Bioeffects of positive and negative acoustic pressures in mice infused with microbubbles. *Ultrasound Med Biol.* 2000; 26: 1327-32.
- Kobayashi N, Yasu T, Yamada S, Kudo N, Kuroki M, Kawakami M, et al. Endothelial cell injury in venule and capillary induced by contrast ultrasonography. *Ultrasound Med Biol.* 2002; 28: 949-56.
- Maruvada S, Hynynen K. Optical monitoring of ultrasound-induced bioeffects in glass catfish. *Ultrasound Med Biol.* 2004; 30: 67-74.
- Miller DL, Gies RA. Gas-body-based contrast agent enhances vascular bioeffects of 1.09 MHz ultrasound on mouse intestine. *Ultrasound Med Biol.* 1998; 24: 1201-8.
- Miller DL, Gies RA. Consequences of lithotripter shockwave interaction with gas body contrast agent in mouse intestine. *J Urol.* 1999; 162: 606-9.
- Miller DL, Gies RA. The influence of ultrasound frequency and gas-body composition on the contrast agent-mediated enhancement of vascular bioeffects in mouse intestine. *Ultrasound Med Biol.* 2000; 26: 307-13.
- Miller DL, Qudus J. Diagnostic ultrasound activation of contrast agent gas bodies induces capillary rupture in mice. *Proc Natl Acad Sci USA.* 2000; 97: 10179-84.
- Price RJ, Skyba DM, Kaul S, Skalak TC. Delivery of colloidal particles and red blood cells to tissue through microvessel ruptures created by targeted microbubble destruction with ultrasound. *Circulation.* 1998; 98: 1264-7.
- Hwang JH, Brayman AA, Reidy MA, Matula TJ, Kimmey MB, Crum LA. Vascular effects induced by combined 1-MHz ultrasound and microbubble contrast agent treatments *in vivo*. *Ultrasound Med Biol.* 2005; 31: 553-64.
- Skyba DM, Price RJ, Linka AZ, Skalak TC, Kaul S. Direct *in vivo* visualization of intravascular destruction of microbubbles by ultrasound and its local effects on tissue. *Circulation.* 1998; 98: 290-3.
- Lu X, Dou C, Fabiilli ML, Miller DL. Capillary Hemorrhage Induced by Contrast-Enhanced Diagnostic Ultrasound in Rat Intestine. *Ultrasound Med Biol.* 2019; 45: 2133-9.
- Dalecki D. WFUMB Safety Symposium on Echo-Contrast Agents: bioeffects of ultrasound contrast agents *in vivo*. *Ultrasound Med Biol.* 2007; 33: 205-13.
- Goertz DE. An overview of the influence of therapeutic ultrasound exposures on the vasculature: High intensity ultrasound and microbubble-mediated bioeffects. *Int J Hyperthermia.* 2015; 31: 134-44.
- Wood AKW, Sehgal CM. A review of low-intensity ultrasound for cancer therapy. *Ultrasound Med Biol.* 2015; 41: 905-28.
- Ho Y-J, Wang T-C, Fan C-H, Yeh C-K. Current progress in antivasular tumor therapy. *Drug Discov Today.* 2017; 22: 1503-15.
- Eisenbrey JR, Forsberg F, Wessner CE, Delaney LJ, Bradigan K, Gummadi S, et al. US-triggered Microbubble Destruction for Augmenting Hepatocellular Carcinoma Response to Transarterial Radioembolization: A Randomized Pilot Clinical Trial. *Radiology.* 2020; 202321.
- Paefgen V, Doleschel D, Kiessling F. Evolution of contrast agents for ultrasound imaging and ultrasound-mediated drug delivery. *Front Pharmacol.* 2015; 6: 249-16.
- Klivanov AL. Ultrasound Contrast: Gas Microbubbles in the Vasculature. *Invest Radiol.* 2021; 56: 50-61.
- Hyvelin J-M, Gaud E, Costa M, Helbert A, Bussat P, Bettinger T, et al. Characteristics and Echogenicity of Clinical Ultrasound Contrast Agents: An *In vitro* and *In vivo* Comparison Study. *J Ultrasound Med.* 2017; 36: 941-53.
- Goertz DE, Jong N de, Steen AFW van der. Attenuation and Size Distribution Measurements of Definity™ and Manipulated Definity™ Populations. *Ultrasound Med Biol.* 2007; 33: 1376-88.
- Bernatik T, Schuler A, Kunze G, Mauch M, Dietrich CF, Dirks K, et al. Benefit of Contrast-Enhanced Ultrasound (CEUS) in the Follow-Up Care of Patients

- with Colon Cancer: A Prospective Multicenter Study. *Ultraschall Med.* 2015; 36: 590-3.
35. Jang H-J, Kim TK, Burns PN, Wilson SR. Enhancement patterns of hepatocellular carcinoma at contrast-enhanced US: comparison with histologic differentiation. *Radiology.* 2007; 244: 898-906.
 36. Zwirn G, Beeri R, Gilon D, Friedman Z, Akselrod S. Quantitative evaluation of local myocardial blood volume in contrast echocardiography. *Med Image Anal.* 2009; 13: 62-79.
 37. Apfel RE. Sonic effervescence: A tutorial on acoustic cavitation. *J Acoust Soc Am.* 1997; 101: 1227-38.
 38. Chomas JE, Dayton P, Allen J, Morgan K, Ferrara KW. Mechanisms of contrast agent destruction. *IEEE Trans Ultrason Ferroelectr Freq Control.* 2001; 48: 232-48.
 39. Kabalnov A, Klein D, Pelura T, Schutt E, Weers J. Dissolution of multicomponent microbubbles in the bloodstream: 1. Theory. *Ultrasound Med Biol.* 1998; 24: 739-49.
 40. Miller DL. Overview of experimental studies of biological effects of medical ultrasound caused by gas body activation and inertial cavitation. *Prog Biophys Mol Biol.* 2007; 93: 314-30.
 41. Choi JJ, Selert K, Vlachos F, Wong A, Konofagou EE. Noninvasive and localized neuronal delivery using short ultrasonic pulses and microbubbles. *Proc Natl Acad Sci USA.* 2011; 108: 16539-44.
 42. Leighton TG. *The acoustic bubble.* London: Academic Press; 1994.
 43. Chen H, Kreider W, Brayman AA, Bailey MR, Matula TJ. Blood vessel deformations on microsecond time scales by ultrasonic cavitation. *Phys Rev Lett.* 2011; 106: 034301.
 44. Hwang JH, Tu J, Brayman AA, Matula TJ, Crum LA. Correlation between inertial cavitation dose and endothelial cell damage *in vivo*. *Ultrasound Med Biol.* 2006; 32: 1611-9.
 45. Burke CW, Klibanov AL, Sheehan JP, Price RJ. Inhibition of glioma growth by microbubble activation in a subcutaneous model using low duty cycle ultrasound without significant heating. *J Neurosurg.* 2011; 114: 1654-61.
 46. Samuel S, Cooper MA, Bull JL, Fowlkes JB, Miller DL. An *ex vivo* study of the correlation between acoustic emission and microvascular damage. *Ultrasound Med Biol.* 2009; 35: 1574-86.
 47. Todorova M, Agache V, Mortazavi O, Chen B, Karshafian R, Hynynen K, et al. Antitumor effects of combining metronomic chemotherapy with the antivasculature action of ultrasound stimulated microbubbles. *Int J Cancer.* 2013; 132: 2956-66.
 48. Goertz DE, Todorova M, Mortazavi O, Agache V, Chen B, Karshafian R, et al. Antitumor effects of combining docetaxel (taxotere) with the antivasculature action of ultrasound stimulated microbubbles. *Woloshchak GE, Ed. PLoS ONE.* 2012; 7: e52307.
 49. Arvanitis CD, Vykhodtseva N, Jolesz F, Livingstone M, McDannold N. Cavitation-enhanced nonthermal ablation in deep brain targets: feasibility in a large animal model. *J Neurosurg.* 2016; 124: 1450-9.
 50. Klotz AR, Lindvere L, Stefanovic B, Hynynen K. Temperature change near microbubbles within a capillary network during focused ultrasound. *Phys Med Biol.* 2010; 55: 1549-61.
 51. Sun T, Zhang Y, Power C, Alexander PM, Sutton JT, Aryal M, et al. Closed-loop control of targeted ultrasound drug delivery across the blood-brain/tumor barriers in a rat glioma model. *Proc Natl Acad Sci USA.* 2017; 114: E10281-90.
 52. O'Reilly MA, Hynynen K. Blood-Brain Barrier: Real-time Feedback-controlled Focused Ultrasound Disruption by Using an Acoustic Emissions-based Controller. *Radiology.* 2012; 263: 96-106.
 53. Arvanitis CD, Livingstone MS, Vykhodtseva N, McDannold N. Controlled ultrasound-induced blood-brain barrier disruption using passive acoustic emissions monitoring. *Munoz-Barrutia A, Ed. PLoS ONE.* 2012; 7: e45783.
 54. Wood AKW, Schultz SM, Lee WM-F, Bunte RM, Sehgal CM. Antivasculature ultrasound therapy extends survival of mice with implanted melanomas. *Ultrasound Med Biol.* 2010; 36: 853-7.
 55. Wang J, Zhao Z, Shen S, Zhang C, Guo S, Lu Y, et al. Selective depletion of tumor neovasculature by microbubble destruction with appropriate ultrasound pressure. *Int J Cancer.* 2015; 137: 2478-91.
 56. Huang P, Zhang Y, Chen J, Shentu W, Sun Y, Yang Z, et al. Enhanced antitumor efficacy of ultrasonic cavitation with up-sized microbubbles in pancreatic cancer. *Oncotarget.* 2015; 6: 20241-51.
 57. Wood AKW, Ansaloni S, Ziemer LS, Lee WM-F, Feldman MD, Sehgal CM. The antivasculature action of physiotherapy ultrasound on murine tumors. *Ultrasound Med Biol.* 2005; 31: 1403-10.
 58. Hu X, Kheiruloomoom A, Mahakian LM, Beegle JR, Kruse DE, Lam KS, et al. Insonation of Targeted Microbubbles Produces Regions of Reduced Blood Flow Within Tumor Vasculature. *Invest Radiol.* 2012; 47: 398-405.
 59. Bunte RM, Ansaloni S, Sehgal CM, Lee WM-F, Wood AKW. Histopathological observations of the antivasculature effects of physiotherapy ultrasound on a murine neoplasm. *Ultrasound Med Biol.* 2006; 32: 453-61.
 60. Stieger SM, Caskey CF, Adamson RH, Qin S, Curry F-RE, Wisner ER, et al. Enhancement of vascular permeability with low-frequency contrast-enhanced ultrasound in the chorioallantoic membrane model. *Radiology.* 2007; 243: 112-21.
 61. Davis C, Fischer J, Ley K, Sarembock IJ. The role of inflammation in vascular injury and repair. *J Thromb Haemost.* 2003; 1: 1699-709.
 62. Chin CT, Raju BI, Shevchenko T, Klibanov AL, 2009. Control and reversal of tumor growth by ultrasound activated microbubbles. In: *IEEE, Ed. 2009. (2009 IEEE International Ultrasonics Symposium).*
 63. Clement GT. Perspectives in clinical uses of high-intensity focused ultrasound. *Ultrasonics.* 2004; 42: 1087-93.
 64. Li Q, Du J, Yu M, He G, Luo W, Li H, et al. Transmission electron microscopy of VX2 liver tumors after high-intensity focused ultrasound ablation enhanced with SonoVue®. *Adv Ther.* 2009; 26: 117-25.
 65. Prosperetti A. Nonlinear oscillations of gas bubbles in liquids. Transient solutions and the connection between subharmonic signal and cavitation. *J Acoust Soc Am.* 1975; 57: 810-21.
 66. Suslick KS, Flannigan DJ. Inside a Collapsing Bubble: Sonoluminescence and the Conditions During Cavitation. *Annu Rev Phys Chem.* 2008; 59: 659-83.
 67. Wood AKW, Bunte RM, Price HE, Deitz MS, Tsai JH, Lee WM-F, et al. The Disruption of Murine Tumor Neovasculature by Low-intensity Ultrasound – Comparison Between 1- and 3-MHz Sonication Frequencies. *Acad Radiol.* 2008; 15: 1133-41.
 68. Levenback BJ, Sehgal CM, Wood AKW. Modeling of thermal effects in antivasculature ultrasound therapy. *J Acoust Soc Am.* 2012; 131: 540-9.
 69. Al-Mahrouki AA, Iradji S, Tran WT, Czarnota GJ. Cellular characterization of ultrasound-stimulated microbubble radiation enhancement in a prostate cancer xenograft model. *Dis Model Mech.* 2014; 7: 363-72.
 70. Czarnota GJ, Karshafian R, Burns PN, Wong S, Mahrouki AA, Lee JW, et al. Tumor radiation response enhancement by acoustical stimulation of the vasculature. *Proc Natl Acad Sci USA.* 2012; 109: E2033-41.
 71. Daecher A, Stanczak M, Liu J-B, Zhang J, Du S, Forsberg F, et al. Localized microbubble cavitation-based antivasculature therapy for improving HCC treatment response to radiotherapy. *Cancer Lett.* 2017; 411: 100-5.
 72. Tran WT, Iradji S, Sofroni E, Giles A, Eddy D, Czarnota GJ. Microbubble and ultrasound radioenhancement of bladder cancer. *Br J Cancer.* 2012; 107: 469-76.
 73. Kwok SJJ, Kaffas AE, Lai P, Mahrouki AA, Lee J, Iradji S, et al. Ultrasound-mediated microbubble enhancement of radiation therapy studied using three-dimensional high-frequency power Doppler ultrasound. *Ultrasound Med Biol.* 2013; 39: 1983-90.
 74. Kaffas AE, Czarnota GJ. Biomechanical effects of microbubbles: from radiosensitization to cell death. *Future Oncol.* 2015; 11: 1093-108.
 75. Kaffas AE, Mahrouki AA, Hashim A, Law N, Giles A, Czarnota GJ. Role of Acid Sphingomyelinase and Ceramide in Mechano-Acoustic Enhancement of Tumor Radiation Responses. *J Natl Cancer Inst.* 2018; 70: 8179.
 76. Nofiele JT, Karshafian R, Furukawa M, Mahrouki AA, Giles A, Wong S, et al. Ultrasound-activated microbubble cancer therapy: ceramide production leading to enhanced radiation effect *in vitro*. *Technol Cancer Res Treat.* 2013; 12: 53-60.
 77. Kaffas AE, Nofiele J, Giles A, Cho S, Liu SK, Czarnota GJ. Dll4-notch signalling blockade synergizes combined ultrasound-stimulated microbubble and radiation therapy in human colon cancer xenografts. *Ramchandran R, Ed. PLoS ONE.* 2014; 9: e93888.
 78. Garcia-Barros M, Paris F, Cordon-Cardo C, Lyden D, Raffii S, Haimovitz-Friedman A, et al. Tumor Response to Radiotherapy Regulated by Endothelial Cell Apoptosis. *Science.* 2003; 300: 1155-9.
 79. Kaffas AE, Gangeh MJ, Farhat G, Tran WT, Hashim A, Giles A, et al. Tumour Vascular Shutdown and Cell Death Following Ultrasound-Microbubble Enhanced Radiation Therapy. *Theranostics.* 2018; 8: 314-27.
 80. Al-Mahrouki AA, Karshafian R, Giles A, Czarnota GJ. Bioeffects of ultrasound-stimulated microbubbles on endothelial cells: gene expression changes associated with radiation enhancement *in vitro*. *Ultrasound Med Biol.* 2012; 38: 1958-69.
 81. Su Z, Xu T, Wang Y, Guo X, Tu J, Zhang D, et al. Low-intensity pulsed ultrasound promotes apoptosis and inhibits angiogenesis via p38 signaling-mediated endoplasmic reticulum stress in human endothelial cells. *Mol Med Rep.* 2019; 19: 4645-54.
 82. Chappell JC, Klibanov AL, Price RJ. Ultrasound-microbubble-induced neovascularization in mouse skeletal muscle. *Ultrasound Med Biol.* 2005; 31: 1411-22.
 83. Song J, Qi M, Kaul S, Price RJ. Stimulation of arteriogenesis in skeletal muscle by microbubble destruction with ultrasound. *Circulation.* 2002; 106: 1550-5.
 84. Burks SR, Nguyen BA, Tebebi PA, Kim SJ, Bresler MN, Ziadloo A, et al. Pulsed Focused Ultrasound Pretreatment Improves Mesenchymal Stromal Cell Efficacy in Preventing and Rescuing Established Acute Kidney Injury in Mice. *Stem Cells.* 2015; 33: 1241-53.
 85. Tebebi PA, Kim SJ, Williams RA, Milo B, Frenkel V, Burks SR, et al. Improving the therapeutic efficacy of mesenchymal stromal cells to restore perfusion in critical limb ischemia through pulsed focused ultrasound. *Sci Rep.* 2017; 7: 41550-11.
 86. Ling Z-Y, Shu S, Zhong S-G, Luo J, Su L, Liu Z-Z, et al. Ultrasound Targeted Microbubble Destruction Promotes Angiogenesis and Heart Function by Inducing Myocardial Microenvironment Change. *Ultrasound Med Biol.* 2013; 39: 2001-10.
 87. Ghanem A, Steingen C, Brenig F, Funcke F, Bai Z-Y, Hall C, et al. Focused ultrasound-induced stimulation of microbubbles augments site-targeted engraftment of mesenchymal stem cells after acute myocardial infarction. *J Mol Cell Cardiol.* 2009; 47: 411-8.

88. McMahon D, Bendayan R, Hynynen K. Acute effects of focused ultrasound-induced increases in blood-brain barrier permeability on rat microvascular transcriptome. *Sci Rep.* 2017; 7: 45657.
89. McMahon D, Mah E, Hynynen K. Angiogenic response of rat hippocampal vasculature to focused ultrasound-mediated increases in blood-brain barrier permeability. *Sci Rep.* 2018; 8: 12178.
90. McMahon D, Hynynen K. Acute Inflammatory Response Following Increased Blood-Brain Barrier Permeability Induced by Focused Ultrasound is Dependent on Microbubble Dose. *Theranostics.* 2018; 7: 3989–4000.
91. Vykhodtseva N, McDannold N, Hynynen K. Induction of apoptosis *in vivo* in the rabbit brain with focused ultrasound and Optison. *Ultrasound Med Biol.* 2006; 32: 1923–9.
92. Kovacs ZI, Kim S, Jikaria N, Qureshi F, Milo B, Lewis BK, et al. Disrupting the blood-brain barrier by focused ultrasound induces sterile inflammation. *Proc Natl Acad Sci USA.* 2017; 114: E75–84.
93. Fujishiro S, Mitsumori M, Nishimura Y, Okuno Y, Nagata Y, Hiraoka M, et al. Increased heating efficiency of hyperthermia using an ultrasound contrast agent: a phantom study. *Int J Hypertherm.* 1998; 14: 495–502.
94. Luo W, Zhou X, Tian X, Ren X, Zheng M, Gu K, et al. Enhancement of ultrasound contrast agent in high-intensity focused ultrasound ablation. *Adv Ther.* 2006; 23: 861–8.
95. Peng S, Xiong Y, Li K, He M, Deng Y, Chen L, et al. Clinical utility of a microbubble-enhancing contrast (“SonoVue”) in treatment of uterine fibroids with high intensity focused ultrasound: a retrospective study. *Eur J Radiol.* 2012; 81: 3832–8.
96. Umemura S, Kawabata K, Hashiba K. Enhancement of Ultrasonic Absorption by Microbubbles for Therapeutic Application. 2001 *IEEE Ultrasonics Symposium Proc Int Symposium (Cat 01ch37263).* 2001; 2: 1311–4.
97. Tran BC, Seo J, Hall TL, Fowlkes JB, Cain CA. Microbubble-Enhanced Cavitation for Noninvasive Ultrasound Surgery. *IEEE Trans Ultrason Ferroelectr Freq Control.* 2003; 50: 1296–304.
98. McDannold NJ, Vykhodtseva NI, Hynynen K. Microbubble contrast agent with focused ultrasound to create brain lesions at low power levels: MR imaging and histologic study in rabbits. *Radiology.* 2006; 241: 95–106.
99. McDannold N, Vykhodtseva N, Jolesz FA, Hynynen K. MRI investigation of the threshold for thermally induced blood-brain barrier disruption and brain tissue damage in the rabbit brain. *Magnet Reson Med.* 2004; 51: 913–23.
100. Vykhodtseva N, Sorrentino V, Jolesz FA, Bronson RT, Hynynen K. MRI detection of the thermal effects of focused ultrasound on the brain. *Ultrasound Med Biol.* 2000; 26: 871–80.
101. McDannold N, Zhang Y, Vykhodtseva N. Nonthermal ablation in the rat brain using focused ultrasound and an ultrasound contrast agent: long-term effects. *J Neurosurg.* 2016; 125: 1539–48.
102. McDannold N, Zhang Y-Z, Power C, Jolesz F, Vykhodtseva N. Nonthermal ablation with microbubble-enhanced focused ultrasound close to the optic tract without affecting nerve function. *J Neurosurg.* 2013; 119: 1208–20.
103. Huang Y, Vykhodtseva NI, Hynynen K. Creating brain lesions with low-intensity focused ultrasound with microbubbles: a rat study at half a megahertz. *Ultrasound Med Biol.* 2013; 39: 1420–8.
104. Lin C-Y, Tseng H-C, Shiu H-R, Wu M-F, Chou C-Y, Lin W-L. Ultrasound sonication with microbubbles disrupts blood vessels and enhances tumor treatments of anticancer nanodrug. *Int J Nanomedicine.* 2012; 7: 2143–52.
105. Curley CT, Sheybani ND, Bullock TN, Price RJ. Focused Ultrasound Immunotherapy for Central Nervous System Pathologies: Challenges and Opportunities. *Theranostics.* 2017; 7: 3608–23.
106. Sheybani ND, Price RJ. Perspectives on Recent Progress in Focused Ultrasound Immunotherapy. *Theranostics.* 2019; 9: 7749–58.
107. Mauri G, Nicosia L, Xu Z, Pietro SD, Monfardini L, Bonomo G, et al. Focused ultrasound: tumour ablation and its potential to enhance immunological therapy to cancer. *Br J Radiol.* 2018; 3: 20170641–9.
108. Hunt SJ, Gade T, Soulen MC, Pickup S, Sehgal CM. Antivasular ultrasound therapy: magnetic resonance imaging validation and activation of the immune response in murine melanoma. *J Ultrasound Med.* 2015; 34: 275–87.
109. Liu H-L, Hsieh H-Y, Lu L-A, Kang C-W, Wu M-F, Lin C-Y. Low-pressure pulsed focused ultrasound with microbubbles promotes an anticancer immunological response. *J Transl Med.* 2012; 10: 221.
110. Bulner S, Prodeus A, Garipey J, Hynynen K, Goertz DE. Enhancing Checkpoint Inhibitor Therapy with Ultrasound Stimulated Microbubbles. *Ultrasound Med Biol.* 2019; 45: 500–12.
111. Bandyopadhyay S, Quinn IJ, Scandiuzzi L, Basu I, Partanen A, Tomé WA, et al. Low-Intensity Focused Ultrasound Induces Reversal of Tumor-Induced T Cell Tolerance and Prevents Immune Escape. *J Immunol.* 2016; 196: 1964–76.
112. Aydin O, Chandran P, Lorsung RR, Cohen G, Burks SR, Frank JA. The Proteomic Effects of Pulsed Focused Ultrasound on Tumor Microenvironments of Murine Melanoma and Breast Cancer Models. *Ultrasound Med Biol.* 2019; 1–14.
113. Baseri B, Choi JJ, Tung Y-S, Konofagou EE. Multi-Modality Safety Assessment of Blood-Brain Barrier Opening Using Focused Ultrasound and Definity Microbubbles: A Short-Term Study. *Ultrasound Med Biol.* 2010; 36: 1445–59.
114. Choi JJ, Coussios C-C. Spatiotemporal evolution of cavitation dynamics exhibited by flowing microbubbles during ultrasound exposure. *J Acoust Soc Am.* 2012; 132: 3538–49.
115. Poulipoulos AN, Li C, Tinguely M, Garbin V, Tang M-X, Choi JJ. Rapid short-pulse sequences enhance the spatiotemporal uniformity of acoustically driven microbubble activity during flow conditions. *J Acoust Soc Am.* 2016; 140: 2469–80.
116. Morse SV, Poulipoulos AN, Chan TG, Copping MJ, Lin J, Long NJ, et al. Rapid Short-pulse Ultrasound Delivers Drugs Uniformly across the Murine Blood-Brain Barrier with Negligible Disruption. *Radiology.* 2019; 181625.
117. McMahon D, Deng L, Hynynen K. Comparing rapid short-pulse to tone burst sonication sequences for focused ultrasound and microbubble-mediated blood-brain barrier permeability enhancement. *J Control Release.* 2020;
118. Wible JH, Galen KP, Wojdyla JK, Hughes MS, Klivanov AL, Brandenburger GH. Microbubbles induce renal hemorrhage when exposed to diagnostic ultrasound in anesthetized rats. *Ultrasound Med Biol.* 2002; 28: 1535–46.
119. Radhakrishnan K, Bader KB, Haworth KJ, Kopeček JA, Raymond JL, Huang S-L, et al. Relationship between cavitation and loss of echogenicity from ultrasound contrast agents. *Phys Med Biol.* 2013; 58: 935–48.
120. Greis C. Quantitative evaluation of microvascular blood flow by contrast-enhanced ultrasound (CEUS). *Clin Hemorheol Microcirc.* 2011; 49: 137–49.
121. Song K-H, Fan AC, Hinkle JJ, Newman J, Borden MA, Harvey BK. Microbubble gas volume: A unifying dose parameter in blood-brain barrier opening by focused ultrasound. *Theranostics.* 2018; 7: 144–52.
122. Sirsi S, Peshitan J, Kwan J, Homma S, Borden M. Effect of microbubble size on fundamental mode high frequency ultrasound imaging in mice. *Ultrasound Med Biol.* 2010; 36: 935–48.
123. Prada F, Mattei L, Bene MD, Aiani L, Saini M, Casali C, et al. Intraoperative Cerebral Glioma Characterization with Contrast Enhanced Ultrasound. *Biomed Res Int.* 2014; 2014: 1–9.
124. Prada F, Perin A, Martegani A, Aiani L, Solbiati L, Lamperti M, et al. Intraoperative Contrast-Enhanced Ultrasound for Brain Tumor Surgery. *Neurosurgery.* 2014; 74: 542–52.
125. Prada F, Bene MD, Casali C, Saladino A, Legnani FG, Perin A, et al. Intraoperative Navigated Angiosonography for Skull Base Tumor Surgery. *World Neurosurg.* 2015; 84: 1699–707.
126. Schneider M. Characteristics of SonoVue™. *Echocardiography.* 1999; 16: 743–6.
127. Kalantarinia K, Okusa MD. Ultrasound contrast agents in the study of kidney function in health and disease. *Drug Discov Today Dis Mech.* 2007; 4: 153–8.
128. Schneider M, Anantharam B, Arditi M, Bokor D, Broillet A, Bussat P, et al. BR38, a new ultrasound blood pool agent. *Invest Radiol.* 2011; 46: 486–94.
129. Caskey CF, Stieger SM, Qin S, Dayton PA, Ferrara KW. Direct observations of ultrasound microbubble contrast agent interaction with the microvessel wall. *J Acoust Soc Am.* 2007; 122: 1191–200.
130. Kim HC, Mahrouki AA, Gorjizadeh A, Karshafian R, Czarnota GJ. Effects of biophysical parameters in enhancing radiation responses of prostate tumors with ultrasound-stimulated microbubbles. *Ultrasound Med Biol.* 2013; 39: 1376–87.
131. Huang Y, Alkins R, Schwartz ML, Hynynen K. Opening the Blood-Brain Barrier with MR Imaging-guided Focused Ultrasound: Preclinical Testing on a Trans-Human Skull Porcine Model. *Radiology.* 2017; 282: 123–30.
132. Prada F, Gennari AG, Linville IM, Mutersbaugh ME, Chen Z, Sheybani N, et al. Quantitative analysis of *in-vivo* microbubble distribution in the human brain. *Sci Rep.* 2021; 11: 11797.
133. Klein J, Tran W, Lai P, Al-Mahrouki A, Giles A, Czarnota GJ. Effect of Treatment Sequencing on the Tumor Response to Combined Treatment With Ultrasound-Stimulated Microbubbles and Radiotherapy. *J Ultras Med.* 2020; 39: 2415–25.
134. Hu Z, Zhang H, Mordovanakis A, Paulus YM, Liu Q, Wang X, et al. High-precision, non-invasive anti-microvascular approach via concurrent ultrasound and laser irradiation. *Sci Rep.* 2017; 7: 40243.
135. Liu H, Zheng T, Zhou Z, Hu A, Li M, Zhang Z, et al. Berberine nanoparticles for promising sonodynamic therapy of a HeLa xenograft tumour. *RSC Adv.* 2019; 9: 10528–35.
136. Li X, Guo S, Xu T, He X, Sun Y, Chen X, et al. Therapeutic ultrasound combined with microbubbles improves atherosclerotic plaque stability by selectively destroying the intraplaque neovasculature. *Theranostics.* 2020; 10: 2522–37.
137. Yang H, Sun Y, Wei J, Xu L, Tang Y, Yang L, et al. The effects of ultrasound-targeted microbubble destruction (UTMD) carrying IL-8 monoclonal antibody on the inflammatory responses and stability of atherosclerotic plaques. *Biomed Pharmacother.* 2019; 118: 109161.
138. Xiao S, Hu Z, He Y, Jin H, Yang Y, Chen L, et al. Enhancement Effect of Microbubble-Enhanced Ultrasound in Microwave Ablation in Rabbit VX2 Liver Tumors. *BioMed Res Int.* 2020; 2020: 1–10.
139. Zhu L, Cheng G, Ye D, Nazeri A, Yue Y, Liu W, et al. Focused Ultrasound-enabled Brain Tumor Liquid Biopsy. *Sci Rep.* 2018; 8: 6553.
140. Pacia CP, Zhu L, Yang Y, Yue Y, Nazeri A, Gach HM, et al. Feasibility and safety of focused ultrasound-enabled liquid biopsy in the brain of a porcine model. *Sci Rep.* 2020; 10: 7449.
141. Zhu L, Nazeri A, Pacia CP, Yue Y, Chen H. Focused ultrasound for safe and effective release of brain tumor biomarkers into the peripheral circulation. *PLoS One.* 2020; 15: e0234182.
142. Meng Y, Pople CB, Suppiah S, Llinas M, Huang Y, Sahgal A, et al. MR-guided focused ultrasound liquid biopsy enriches circulating biomarkers in patients with brain tumors. *Neuro Oncol.* 2021;

143. Gorick CM, Mathew AS, Garrison WJ, Thim EA, Fisher DG, Copeland CA, et al. Sonoselective transfection of cerebral vasculature without blood-brain barrier disruption. *Proc Natl Acad Sci USA*. 2020; 23: 201914595–11.
144. Santos MA, Wu S-K, Li Z, Goertz DE, Hynynen K. Microbubble-assisted MRI-guided focused ultrasound for hyperthermia at reduced power levels. *Int J Hyperther*. 2018; 35: 1–13.
145. Dimceviski G, Kotopoulos S, Bjånes T, Hoem D, Schjøtt J, Gjertsen BT, et al. A human clinical trial using ultrasound and microbubbles to enhance gemcitabine treatment of inoperable pancreatic cancer. *J Control Release*. 2016; 243: 172–81.
146. Stride E, Segers T, Lajoie G, Cherkaoui S, Bettinger T, Versluis M, et al. Microbubble Agents: New Directions. *Ultrasound Med Biol*. 2020; 46: 1326–43.
147. Lea-Banks H, O'Reilly MA, Hynynen K. Ultrasound-responsive droplets for therapy: A review. *J Control Release*. 2019; 293: 144–54.
148. Lin C-Y, Pitt WG. Acoustic droplet vaporization in biology and medicine. *BioMed Research Int*. 2013; 404361–13.
149. Kripfgans OD, Orifici CM, Carson PL, Ives KA, Eldevik OP, Fowlkes JB. Acoustic droplet vaporization for temporal and spatial control of tissue occlusion: a kidney study. *IEEE Transactions: Ultrasonics, Ferroelectrics and Frequency Control*. 2005; 52: 1101–10.
150. Zhang M, Fabiilli ML, Haworth KJ, Fowlkes JB, Kripfgans OD, Roberts WW, et al. Initial Investigation of Acoustic Droplet Vaporization for Occlusion in Canine Kidney. *Ultrasound Med Biol*. 2010; 36: 1691–703.
151. Kwan JJ, Myers R, Coviello CM, Graham SM, Shah AR, Stride E, et al. Ultrasound-Propelled Nanocups for Drug Delivery. *Small*. 2015; 11: 5305–14.
152. Mannaris C, Bau L, Grundy M, Gray M, Lea-Banks H, Seth A, et al. Microbubbles, nanodroplets and gas-stabilizing solid particles for ultrasound-mediated extravasation of unencapsulated drugs: an exposure parameter optimization. *Ultrasound Med Biol*. 2019; 45: 954–67.
153. Frinking P, Segers T, Luan Y, Tranquart F. Three Decades of Ultrasound Contrast Agents: A Review of the Past, Present and Future Improvements. *Ultrasound Med Biol*. 2020; 46: 892–908.
154. Rouviere O, Glas L, Girouin N, Mege-Lechevallier F, Gelet A, Dantony E, et al. Prostate Cancer Ablation with Transrectal High-Intensity Focused Ultrasound: Assessment of Tissue Destruction with Contrast-enhanced US. *Radiology*. 2011; 259: 583–91.
155. Rouviere O, Gelet A, Crouzet S, Chapelon J-Y. Prostate focused ultrasound focal therapy—imaging for the future. *Nat Rev Clin Oncol*. 2012; 9: 721–7.
156. Gessner R, Lukacs M, Lee M, Cherin E, Foster FS, Dayton PA. High-resolution, high-contrast ultrasound imaging using a prototype dual-frequency transducer: *in vitro* and *in vivo* studies. *IEEE Transactions Ultrasonics Ferroelectr Freq Control*. 2010; 57: 1772–81.
157. Gessner RC, Aylward SR, Dayton PA. Mapping Microvasculature with Acoustic Angiography Yields Quantifiable Differences between Healthy and Tumor-bearing Tissue Volumes in a Rodent Model. *Radiology*. 2012; 264: 733–40.
158. Gessner RC, Frederick CB, Foster FS, Dayton PA. Acoustic angiography: a new imaging modality for assessing microvasculature architecture. *Int J Biomed Imaging*. 2013; 2013: 936593.
159. Errico C, Pierre J, Pezet S, Desailly Y, Lenkei Z, Couture O, et al. Ultrafast ultrasound localization microscopy for deep super-resolution vascular imaging. *Nature*. 2015; 527: 499–502.
160. Christensen-Jeffries K, Couture O, Dayton PA, Eldar YC, Hynynen K, Kiessling F, et al. Super-resolution Ultrasound Imaging. *Ultrasound Med Biol*. 2020; 46: 865–91.
161. Opacic T, Dencks S, Theek B, Piepenbrock M, Ackermann D, Rix A, et al. Motion model ultrasound localization microscopy for preclinical and clinical multiparametric tumor characterization. *Nat Commun*. 2018; 9: 1527.
162. Yang Yu, Bai W, Chen Y, Lin Y, Hu B. Optimization of low-frequency low-intensity ultrasound-mediated microvessel disruption on prostate cancer xenografts in nude mice using an orthogonal experimental design. *Oncol Lett*. 2015; 10: 2999–37.
163. Liu Z, Gao S, Zhao Y, Li P, Liu J, Li P, et al. Disruption of Tumor Neovasculature by Microbubble Enhanced Ultrasound: A Potential New Physical Therapy of Anti-Angiogenesis. *Ultrasound Med Biol*. 2012; 38: 253–1.